

University of Groningen

## WO<sub>3</sub>-SiO<sub>2</sub> nanomaterials synthesized using a novel template-free method in supercritical CO<sub>2</sub> as heterogeneous catalysts for epoxidation with H<sub>2</sub>O<sub>2</sub>

Tao, Yehan; De Luca, Oreste; Singh, Bhawan; Kamphuis, Aeilke J.; Chen, Juan; Rudolf, Petra; Pescarmona, Paolo P.

*Published in:*  
Materials Today Chemistry

*DOI:*  
[10.1016/j.mtchem.2020.100373](https://doi.org/10.1016/j.mtchem.2020.100373)

**IMPORTANT NOTE: You are advised to consult the publisher's version (publisher's PDF) if you wish to cite from it. Please check the document version below.**

*Document Version*  
Publisher's PDF, also known as Version of record

*Publication date:*  
2020

[Link to publication in University of Groningen/UMCG research database](#)

### *Citation for published version (APA):*

Tao, Y., De Luca, O., Singh, B., Kamphuis, A. J., Chen, J., Rudolf, P., & Pescarmona, P. P. (2020). WO<sub>3</sub>-SiO<sub>2</sub> nanomaterials synthesized using a novel template-free method in supercritical CO<sub>2</sub> as heterogeneous catalysts for epoxidation with H<sub>2</sub>O<sub>2</sub>. *Materials Today Chemistry*, 18, [100373]. <https://doi.org/10.1016/j.mtchem.2020.100373>

### **Copyright**

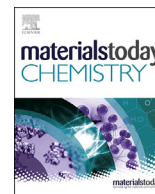
Other than for strictly personal use, it is not permitted to download or to forward/distribute the text or part of it without the consent of the author(s) and/or copyright holder(s), unless the work is under an open content license (like Creative Commons).

The publication may also be distributed here under the terms of Article 25fa of the Dutch Copyright Act, indicated by the "Taverne" license. More information can be found on the University of Groningen website: <https://www.rug.nl/library/open-access/self-archiving-pure/taverne-amendment>.

### **Take-down policy**

If you believe that this document breaches copyright please contact us providing details, and we will remove access to the work immediately and investigate your claim.

Downloaded from the University of Groningen/UMCG research database (Pure): <http://www.rug.nl/research/portal>. For technical reasons the number of authors shown on this cover page is limited to 10 maximum.



# WO<sub>3</sub>–SiO<sub>2</sub> nanomaterials synthesized using a novel template-free method in supercritical CO<sub>2</sub> as heterogeneous catalysts for epoxidation with H<sub>2</sub>O<sub>2</sub>

Yehan Tao<sup>a</sup>, Oreste De Luca<sup>b</sup>, Bhawan Singh<sup>a</sup>, Aeilke J. Kamphuis<sup>a</sup>, Juan Chen<sup>c</sup>,  
Petra Rudolf<sup>b</sup>, Paolo P. Pescarmona<sup>a,\*</sup>

<sup>a</sup> Chemical Engineering Group, Engineering and Technology Institute Groningen (ENTEG), Faculty of Science and Engineering, University of Groningen, the Netherlands

<sup>b</sup> Zernike Institute for Advanced Materials, Faculty of Science and Engineering, University of Groningen, the Netherlands

<sup>c</sup> Stratingh Institute for Chemistry, Faculty of Science and Engineering, University of Groningen, the Netherlands



## ARTICLE INFO

### Article history:

Received 22 July 2020

Received in revised form

14 September 2020

Accepted 16 September 2020

Available online xxx

### Keywords:

WO<sub>3</sub>–SiO<sub>2</sub> materials

Supercritical CO<sub>2</sub>-assisted catalyst synthesis

Heterogeneous catalysis

Alkene epoxidation

Reactor design

## ABSTRACT

A series of tungsten oxide-silica (WO<sub>3</sub>–SiO<sub>2</sub>) composite nanomaterials were synthesized through a novel, template-free sol-gel method, in which supercritical-CO<sub>2</sub> (scCO<sub>2</sub>) was utilized as synthesis medium. The efficacy of the synthesis method stems from a tailored reactor design that allows the contact of the reactants only in the presence of scCO<sub>2</sub>. Selected synthetic parameters were screened with the purpose of enhancing the performance of the resulting materials as heterogeneous catalysts in epoxidation reactions with H<sub>2</sub>O<sub>2</sub> as environmentally friendly oxidant. A cyclooctene conversion of 73% with epoxide selectivity of > 99% was achieved over the best WO<sub>3</sub>–SiO<sub>2</sub> catalyst under mild reaction conditions (80 °C), equimolar H<sub>2</sub>O<sub>2</sub> amount (1:1) and low WO<sub>3</sub> loading (~2.5 wt%). The turnover number achieved with this catalyst (TON = 328), is significantly higher than that of a WO<sub>3</sub>–SiO<sub>2</sub> prepared via a similar sol-gel route but without supercritical CO<sub>2</sub>, and that of commercial WO<sub>3</sub>. A thorough characterization with a combination of techniques (ICP-OES, N<sub>2</sub>-physisorption, XRD, TEM, STEM-EDX, SEM-EDX, FT-IR and Raman spectroscopy, XPS, TGA and FT-IR analysis of adsorbed pyridine) allowed correlating the physicochemical properties of the WO<sub>3</sub>–SiO<sub>2</sub> nanomaterials with their catalytic performance. The high catalytic activity was attributed to: (i) the very high surface area (892 m<sup>2</sup>/g) and (ii) good dispersion of the W species acting as Lewis acid sites, which were both brought about by the synthesis in supercritical CO<sub>2</sub>, and (iii) the relatively low hydrophilicity, which was tuned by optimizing the tetramethyl ortho-silicate concentration and the amount of basic solution used in the synthesis of the materials. Our optimum catalyst was also tested in the reaction of cyclohexene with H<sub>2</sub>O<sub>2</sub>, resulting in cyclohexane diol as main product due to the presence of strong Brønsted acid sites in the catalyst, whereas the reaction with limonene yielded the internal epoxide as the major product and the corresponding diol as side product. Importantly, the catalyst did not show leaching and could be reused in five consecutive runs without any decrease in activity.

© 2020 The Authors. Published by Elsevier Ltd. This is an open access article under the CC BY license (<http://creativecommons.org/licenses/by/4.0/>).

## 1. Introduction

Epoxides are very important chemicals in organic synthesis, because they are employed in the preparation of a broad range of useful products such as epoxy glues, coatings, surfactants, lubricants, plasticizers, flavors for food, cosmetics and pharmaceuticals

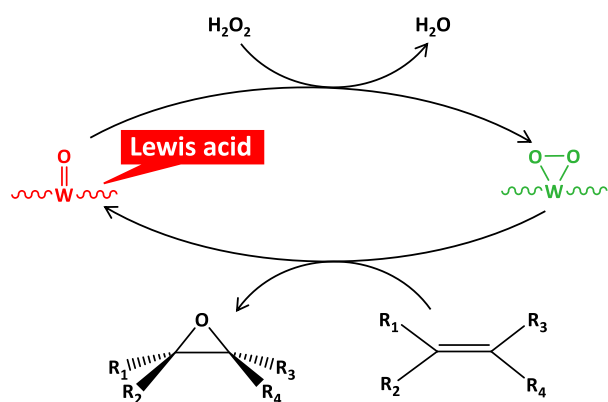
[1–3]. Hydrogen peroxide (H<sub>2</sub>O<sub>2</sub>) is a suitable oxidant for synthesizing epoxides from unsaturated compounds in terms of environmental and economic considerations, because it has a high active oxygen content and generates water as the only by-product [4]. Many metal-based catalytic systems have been developed, in which metallic centers act as acid sites or redox sites, which are responsible for the activation of H<sub>2</sub>O<sub>2</sub> towards the epoxidation reaction [5,6]. Various mechanisms have been proposed for metal-catalyzed epoxidations with H<sub>2</sub>O<sub>2</sub>, which can involve the

\* Corresponding author.

E-mail address: [p.p.pescarmona@rug.nl](mailto:p.p.pescarmona@rug.nl) (P.P. Pescarmona).

formation of different intermediates (metal-peroxo, metal-hydroperoxo or metal-oxo species) and which can proceed through non-radical or radical pathways (the two might occur alternatively or competitively) [3,7,8]. Among these metal-based catalysts, Ti-based catalysts have been the most widely studied [9–12]. Microporous Ti-based catalysts like TS-1 are only effective in the epoxidation of relatively small, mostly linear substrates with  $H_2O_2$  as the oxidant, while mesoporous Ti-based catalysts are generally reported to be more efficient with an organic oxidant (e.g. *tert*-butyl hydroperoxide) [13], though can perform well also with  $H_2O_2$  if the hydrophobicity of their surface is enhanced [14]. Tungsten-based materials are another class of epoxidation catalysts that has been growingly investigated in recent years [8,15–17]. Tungsten-catalysts exist in many forms, both as homogeneous (e.g. poly-oxotungstate [18,19], poly-oxoperoxotungstate [20], lacunary poly-oxotungstate [21], transition-metal-substituted poly-oxotungstate [22]) and heterogeneous catalysts (e.g. supported W species [16,17], bulk  $WO_3$  [23]). Most W-based epoxidation catalysts are reported to follow a non-radical pathway, in which the W center acts as a Lewis acid site that activates  $H_2O_2$  through the formation of a peroxo intermediate. The following step is the transfer of the oxygen atom to the alkene, leading to the formation of the epoxide product, as illustrated in Scheme 1 [7,8].

In recent years, increasing research efforts have focused on overcoming the inherent limitations related to the separation of homogeneous W-based epoxidation catalysts. For this purpose, heterogeneous analogs of these tungsten-based homogeneous catalysts have been synthesized and tested [16,17,23]. However, leaching of active W species in the presence of  $H_2O_2$  is a major limitation of many claimed W-based heterogeneous catalysts [17]. Different approaches have been explored to tackle this issue, typically involving immobilization of the W-based active species into or onto high surface area materials, thereby stabilizing them e.g. through W–O–Si covalent bonds [24–26]. Another approach consists in preparing nanoparticulate  $WO_3$  by flame spray pyrolysis. The procedure involves the pyrolysis of metal precursors within a combustible solvent by flame spray at high temperature (flame  $T > 727^\circ C$  when oxygen is used) [27]. The obtained nanoparticulate  $WO_3$  displayed remarkably high activity as heterogeneous catalyst for the epoxidation of cyclooctene and could be reused without loss of activity [23], possibly pointing to a low tendency of these nanoparticles to aggregate. However, their small size hampers their separation and recovery. Therefore, in view of a perspective upscaling and industrial application, the immobilization of W species in a high surface area matrix seems a more viable option. In



**Scheme 1.** General reaction scheme for the epoxidation of alkenes with  $H_2O_2$  over tungsten-based catalysts.

this context, a commonly used approach consists in grafting W species onto an already-synthesized high surface area support (typically ordered porous silica materials, e.g. MCM-48, SBA-15) [28–32]. The obtained  $WO_3$ -MCM-48,<sup>28</sup>  $WO_3$ -SBA-15<sup>29</sup> catalysts showed no leaching in cyclooctene epoxidation with  $H_2O_2$ , though the tests were carried out at relative low reaction temperature ( $30$ – $40^\circ C$ ). The stability of the W species against higher reaction temperature was not addressed. Recently, a W/SiO<sub>2</sub> catalyst prepared by grafting of tungsten species on silica by dry impregnation was reported to show good catalytic performance, no leaching but moderate reusability in the epoxidation of limonene and methyl oleate in the presence of  $H_2O_2$  [32]. An alternative approach involves the coprecipitation of W species with silicon precursors such as tetramethyl orthosilicate (TMOS) or tetraethyl orthosilicate (TEOS), typically in the presence of a surfactant, e.g. Pluronic 123 (P123) [26,33], cetyltrimethylammonium bromide (CTABr) [25,34], or cetyltrimethylammonium chloride (CTACl) [35]. The expected formation of W–O–Si bonds in this coprecipitation process has been proposed to avert the leaching problem of W species. For example, a  $WO_3$ -SiO<sub>2</sub> foam material prepared using P123 as template demonstrated good stability up to  $60^\circ C$  in cycloocta-1,5-diene epoxidation [26], while tungsten-modified silica synthesized with CTABr as template was stable at  $80^\circ C$  in styrene epoxidation [25]. In addition, there are also reports on non-hydrolytic coprecipitation procedures that do not require the use of a surfactant while still resulting in materials with high specific surface area ( $680$ – $780\text{ m}^2/\text{g}$ ) [36]. The prepared W–SiO<sub>2</sub> materials were tested as catalysts for gas-phase metathesis reactions, whereas their catalytic performance and stability in liquid phase reactions (e.g. epoxidations with  $H_2O_2$ ) were not addressed [36].

Most of the aforementioned grafting and coprecipitation methods involve the use of surfactants as templates to create porous structures with high specific surface area ( $> 700\text{ m}^2/\text{g}$ ) [34,37]. Most surfactants are expensive and typically they are not reusable as they are removed by high temperature calcination, thus limiting the large-scale application of these approaches. Additionally, in both the grafting and coprecipitation methods it is difficult to obtain a uniform dispersion of the W-species and thus to prevent the formation of relatively large tungsten oxide particles, which generally implies a decrease in catalytic activity and an increase in leaching issues [23,26].

On this backdrop, developing a template-free synthesis method for active and stable  $WO_3$ -SiO<sub>2</sub> with high surface area and good dispersion of W species is highly desirable. In this work, we present a novel supercritical carbon dioxide (scCO<sub>2</sub>)-assisted sol-gel method to prepare  $WO_3$ -SiO<sub>2</sub> nanomaterials with enhanced activity in the epoxidation of alkenes with  $H_2O_2$ . Sol-gel methods provide a straightforward alternative to template methods, due to their high degree of versatility towards precursors, their mild reaction conditions and easy scale-up [38].  $WO_3$ -SiO<sub>2</sub> composites have been successfully synthesized by template-free sol-gel methods [25,39–42]. Combining sol-gel methods with drying of the gel in supercritical CO<sub>2</sub> has been reported to yield  $WO_3$ -SiO<sub>2</sub> aerogels ( $1.3\text{ wt}\% WO_3$ ) with remarkably high specific surface areas ( $1434\text{ m}^2/\text{g}$  after thermal treatment at  $200^\circ C$  and  $528\text{ m}^2/\text{g}$  after thermal treatment at  $500^\circ C$ ) [43]. Similarly,  $WO_3$ ,  $WO_3$ -Al<sub>2</sub>O<sub>3</sub> and  $WO_3$ -SiO<sub>2</sub>-Al<sub>2</sub>O<sub>3</sub> aerogels were synthesized by a sol-gel route followed by scCO<sub>2</sub>-drying [44]. These methods exploit the negligible surface tension and ease of separation of supercritical CO<sub>2</sub> to generate high surface area materials [38]. However, the dispersion of tungsten species cannot be adjusted in scCO<sub>2</sub>-drying methods. Here, we present a new synthetic strategy in which scCO<sub>2</sub> is not employed as drying agent, but as a solvent. The novelty of this approach lies in the tailored reactor design (Fig. 1, see Experimental section for details), which allows the W and Si precursors and the

base to come in contact, and thus to form the  $\text{WO}_3\text{-SiO}_2$  materials, only in the presence of the  $\text{scCO}_2$  medium. This strategy allows exploiting also other features of supercritical  $\text{CO}_2$  such as its high diffusivity and solvating power [38], to promote the formation of  $\text{WO}_3\text{-SiO}_2$  nanomaterials with high dispersion of W species and with high specific surface area. The prepared materials displayed high activity as heterogeneous catalysts for the epoxidation of alkenes with  $\text{H}_2\text{O}_2$  as the oxidant.

## 2. Materials and methods

### 2.1. Materials

Tungsten (VI) oxychloride ( $\text{WOCl}_4$ , 98.0%), sodium ethoxide solution (21 wt%, ethanol as solvent) and absolute ethanol were used for the preparation of the W precursor for the sol-gel synthesis of  $\text{WO}_3\text{-SiO}_2$  in  $\text{scCO}_2$  and of the reference material prepared without  $\text{scCO}_2$ . Tetramethyl orthosilicate (TMOS, 98%) was used as the Si precursor. 25 wt% ammonia aqueous solution was used as the water and base source in the sol-gel process. Commercially available  $\text{WO}_3$  ( $\text{WO}_3\text{-Comm}$ ) was used as a reference catalyst. In epoxidation reactions, *cis*-cyclooctene (95%), cyclohexene (99%) and (R)-(+)-limonene (98%) were used as substrates, while aqueous  $\text{H}_2\text{O}_2$  (50 wt%) and anhydrous  $\text{H}_2\text{O}_2$  (26 wt% in ethyl acetate, prepared by ourselves) were employed as oxidant. Ethyl acetate (99.8%), 1,4-dioxane (99.8%, stabilized), 1,3-dioxolane (99%, stabilized), acetonitrile (99.8%), isopropanol (99.5%), ethanol (100%) and methanol (100%) were tested as reaction solvents. 2,2,6,6-Tetramethyl-1-piperidinyloxy (TEMPO) was used as radical scavenger. Cerium sulfate [ $\text{Ce}(\text{SO}_4)_2$ ] aqueous solution (0.1 M) was used in the titration of  $\text{H}_2\text{O}_2$ . The ammonia aqueous solution was purchased from Boom, while all the other compounds were purchased from Sigma-Aldrich. All reagents were used without further purification.

### 2.2. $\text{scCO}_2$ -assisted sol-gel synthesis of $\text{WO}_3\text{-SiO}_2$ materials

The  $\text{WO}_3\text{-SiO}_2$  materials were prepared using a  $\text{scCO}_2$ -assisted sol-gel method with a novel protocol developed by adapting the synthesis methods of other metal oxides in  $\text{scCO}_2$  medium [38,45–48] and by applying them to a sol-gel method inspired by those used in the literature to prepare  $\text{WO}_3\text{-SiO}_2$  [43,44]. In order to exploit  $\text{scCO}_2$  as reaction medium, we designed a reactor set-up that allows bringing the precursors in contact with each other only during the pressurization to reach  $\text{scCO}_2$  conditions. The reactor set-up is based on the use of an in-house developed glass vessel equipped with two cups fixed on the inner wall of the vessel, a magnetic stirring bar and a screw cap containing a silicone/polytetrafluoroethylene (PTFE) septum (Fig. S1A). The synthesis of the  $\text{WO}_3\text{-SiO}_2$  materials was performed in a high-throughput  $\text{scCO}_2$

reactor unit constructed by Integrated Lab Solutions GmbH (ILS), which contains two modules: (1) a batch reactor equipped with a borosilicate glass window to allow monitoring the reaction visually; and (2) a block containing 10 individually stirred batch reactors, which allows performing 10 reactions simultaneously (Fig. S1A). The two modules can be operated separately or used simultaneously. Each batch reactor has a volume of 84 mL with 30 mm internal diameter and can be operated in a pressure range of 1–200 bar and a temperature range of 20–200 °C. The customized glass vessel described above was designed to fit into these batch reactors (see Fig. S1A). The reactors were pressurized by means of an ISCO pump, heated with electric heating elements and cooled with a water circulation system. Each reactor is equipped with a rupture disk to prevent the risk of overpressure.

We aimed at preparing  $\text{WO}_3\text{-SiO}_2$  materials with 2.0 wt% W loading (corresponding to 2.5 wt%  $\text{WO}_3$  loading). The  $\text{WO}_3\text{-SiO}_2$  materials prepared in this work differ in terms of synthesis parameters. The theoretical yield in the synthesis of all these  $\text{WO}_3\text{-SiO}_2$  materials was set to 300.0 mg. The amounts of precursors were calculated based on these general settings. The synthesis of all  $\text{WO}_3\text{-SiO}_2$  materials started with the preparation of the W precursor ( $\text{WO}(\text{OEt})_4$  in ethanol), following a reported protocol [44]. Briefly,  $\text{WOCl}_4$  (11.4 mg) was weighed in a glass vessel equipped with a magnetic stirring bar and a screw cap containing a silicone/PTFE septum in a glove box under  $\text{N}_2$  atmosphere because of its highly hygroscopic nature. Then, a 21 wt% solution of sodium ethoxide in ethanol (41.5 mg) and absolute ethanol (240.0 mg) were mixed under a fume hood, and this solution was added dropwise with a syringe needle to the closed vessel containing  $\text{WOCl}_4$  under continuous stirring. NaCl was formed as a white solid product, as a consequence of the concomitant formation of  $\text{WO}(\text{OEt})_4$ . After stirring at room temperature for 2 h, the NaCl precipitate was removed by centrifugation (4000 rpm, 20 min) and the supernatant ethanol solution containing  $\text{WO}(\text{OEt})_4$  was labeled as W-prec. In aqueous sol-gel processes, the reactivity of tungsten ethoxide with water is much higher than that of silicon alkoxides, thus tending to generate separate  $\text{WO}_3$  and  $\text{SiO}_2$  phases [43]. To avoid this, in this work the most reactive silicon alkoxide (*i.e.* TMOS) was chosen as Si precursor and prehydrolyzed, with the purpose of compensating as much as possible for the difference in hydrolysis rate between W and Si precursors. A similar prehydrolysis strategy has been reported for the preparation of  $\text{WO}_3\text{-Al}_2\text{O}_3$  or  $\text{WO}_3\text{-Al}_2\text{O}_3\text{-SiO}_2$  [44] and  $\text{V}_2\text{O}_5\text{-TiO}_2$  [49]. The prehydrolysis step involved the dissolution of TMOS (756.0 mg, 4.875 mmol) in ethanol, followed by addition of a 25 wt% aqueous solution of ammonia (referred to as 'basic solution'). The amounts of ethanol and basic solution were tuned using a systematic approach (see Table 1) with the purpose of optimizing the synthesis of the  $\text{WO}_3\text{-SiO}_2$  materials towards their activity as epoxidation

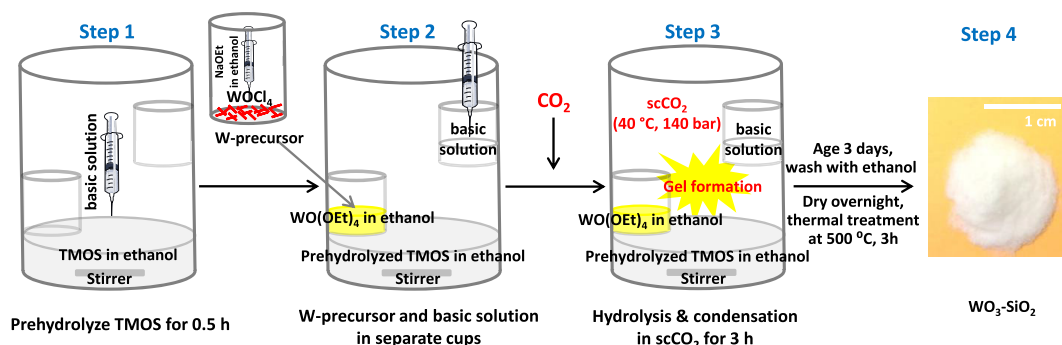


Fig. 1. Scheme of the synthesis of  $\text{WO}_3\text{-SiO}_2$  materials by  $\text{scCO}_2$ -assisted sol-gel method in a customized glass vessel (the cap of the vessel is not shown).

catalysts. Three ethanol amounts were used, *i.e.* 4284.0 mg, 3024.0 mg, and 2268.0 mg, corresponding to 15 wt%, 20 wt%, and 25 wt% TMOS in ethanol. Four basic solution amounts were employed, *i.e.* 86.0 mg, 172.0 mg, 258.0 mg, and 344.0 mg. The obtained mixture, referred to as Si-prec, varied in appearance from a clear solution to an opaque sol as a function of the amounts of ethanol and basic solution employed. The Si-prec mixture was prepared at the bottom of the customized vessel (see Fig. 1, step 1) and stirred (800 rpm) at room temperature for 30 min. Next, an equal amount of basic solution as that used for the prehydrolysis of TMOS was weighed and transferred with a syringe needle to the upper cup of the vessel. Then, W-prec was transferred to the lower cup of the vessel. The septum of the vessel was pierced with two syringe needles to allow CO<sub>2</sub> to flow in and out of the vessel. Then, the vessels were placed into the batch reactors, the block was subsequently closed and stirring (800 rpm) was started immediately. Next, the reactors were firstly pressurized with CO<sub>2</sub> to 60 bar, then heated up to 40 °C, followed by a second pressurization with CO<sub>2</sub> to 140 bar (this process takes around 1.5 h). The applied conditions are above the critical point of CO<sub>2</sub> (T<sub>c</sub> = 31.1 °C, p<sub>c</sub> = 7.38 MPa). During this pressurization step, the mixtures placed in the different compartments of our customized vessel are brought in contact with each other (as visually monitored when the experiments were carried out in the reactor with the borosilicate glass window). After reaching these conditions, the reaction mixtures were continuously stirred for 3 h. Next, the stirring was stopped, the block was cooled down to 20 °C and CO<sub>2</sub> was removed slowly with an average depressurization rate of 1.5 bar/min. The whole procedure described above takes 8–9 h. After reaching atmospheric pressure, the obtained mixtures were aged in the original vessels for 3 days. Then, they were washed thoroughly with ethanol for three times under centrifugation (4000 rpm, 20 min), followed by drying at 80 °C for 12 h and thermal treatment in a calcination oven at 500 °C for 3 h (heating rate: 3 °C/min). This calcination temperature is only slightly above the temperature (450 °C) at which amorphous WO<sub>3</sub> starts to convert into the crystalline form [50]. The whole preparation procedure is summarized in Fig. 1. The synthesized WO<sub>3</sub>–SiO<sub>2</sub> materials were named as WO<sub>3</sub>–xSiO<sub>2</sub>–y, where x is the wt% of TMOS in ethanol used as Si precursor (x = 15, 20, 25) and y is the molar ratio between ammonia and Si + W (y = 0.25, 0.5, 0.75, 1).

A reference WO<sub>3</sub>–SiO<sub>2</sub> material (WO<sub>3</sub>–SiO<sub>2</sub>–Ref) was synthesized with a similar procedure to that used to prepare WO<sub>3</sub>–20SiO<sub>2</sub>–0.5 (our optimum catalyst), but without the use of scCO<sub>2</sub>. Briefly,

the preparation of the W precursor was the same as that for WO<sub>3</sub>–20SiO<sub>2</sub>–0.5. Then, 756.0 mg TMOS was dissolved in 3024.0 mg ethanol upon stirring in a round-bottom flask. Then, 172 mg of the 25 wt% aqueous solution of ammonia was added to the solution and the reaction mixture was stirred at room temperature for 30 min. Next, the reaction mixture was heated up to 40 °C. Afterwards, the W precursor and 172 mg of the 25 wt% aqueous solution of ammonia were added dropwise with separate syringe needles to the prehydrolyzed TMOS in 30 min under continuous stirring. After stirring at 40 °C for 3 h, the obtained mixture was cooled down, aged, washed, dried, and thermally treated following the same procedure used for WO<sub>3</sub>–20SiO<sub>2</sub>–0.5. Another reference catalyst with 1.3 wt% WO<sub>3</sub> was also synthesized (see Supporting Information).

### 2.3. Characterization

Elemental analysis was carried out by inductively coupled plasma optical emission spectroscopy (ICP-OES) on a Perkin Elmer Optima 7000 DV instrument. Before the analysis, the samples were dissolved using a mixture of hydrofluoric acid (HF) and nitric acid (HNO<sub>3</sub>). N<sub>2</sub>-physisorption isotherms were recorded on a Micromeritics ASAP 2420 apparatus at –196 °C. The samples were degassed under reduced pressure (≤ 133 μbar) at 200 °C for 5 h before N<sub>2</sub> adsorption. The specific surface area was evaluated with the Brunauer–Emmett–Teller (BET) method. It should be noted that the measurement of the specific surface area typically has an intrinsic experimental error of about 5%. X-ray diffraction patterns (XRD) were recorded on a Bruker D8 Phaser diffractometer operated with Cu Kα radiation (λ = 1.5406 Å). XRD patterns were measured in reflection geometry in the 2θ range between 10 and 80° with 0.02° and a counting time of 0.5 s for each step. Transmission electron microscopy (TEM) images were collected on a Philips CM12 microscope operating at 120 keV. The scanning transmission electron microscopy (STEM) and energy-dispersive X-ray (EDX) spectroscopy mapping were carried out on an FEI Tecnai T20 electron microscope operating at 200 keV, equipped with an X-Max 80T SDD detector (Oxford Instruments). For the preparation of the TEM/STEM samples, the powder sample was dispersed in ethanol by sonication for 20 min and then deposited on a holey carbon-coated copper grid. Scanning electron microscopy (SEM) and SEM-EDX analysis was performed on a Philips XL30 ESEM microscope operating at 20 keV. The SEM samples were prepared by dispersing the powder sample on a carbon tape and gold was

**Table 1**  
Selected physicochemical properties and catalytic performance of WO<sub>3</sub>–SiO<sub>2</sub> materials prepared with different synthetic parameters.

Entry	Catalyst	Synthesis			Physicochemical properties			Catalytic performance <sup>a</sup>		
		TMOS Conc. (wt%)	Base/(W + Si) ratio	Yield of Catalyst Synthesis (%)	W (wt%) <sup>b</sup>	Specific surface area (m <sup>2</sup> /g)	Adsorbed H <sub>2</sub> O (nH <sub>2</sub> O/nm <sup>2</sup> )	Alkene Conv. (%)	Epoxide Yield (%)	TON <sup>c</sup>
1	WO <sub>3</sub> –15SiO <sub>2</sub> –0.25	15	0.25	> 40	4.8	–	–	62	60	115
2	WO <sub>3</sub> –15SiO <sub>2</sub> –0.5	15	0.5	> 90	2.0	642	5.8	36	36	169
3	WO <sub>3</sub> –15SiO <sub>2</sub> –0.75	15	0.75	> 90	1.8	723	14.8	27	27	139
4	WO <sub>3</sub> –15SiO <sub>2</sub> –1	15	1	> 90	2.1	609	19.1	25	25	108
5	WO <sub>3</sub> –20SiO <sub>2</sub> –0.25	20	0.25	~ 50	3.5	–	–	67	63	165
6	WO <sub>3</sub> –20SiO <sub>2</sub> –0.5	20	0.5	> 90	2.1	892	3.1	62	62	278
7	WO <sub>3</sub> –20SiO <sub>2</sub> –0.75	20	0.75	> 90	2.0	1074	4.1	44	44	201
8	WO <sub>3</sub> –20SiO <sub>2</sub> –1	20	1	> 90	1.8	315	13.0	43	43	216
9	WO <sub>3</sub> –25SiO <sub>2</sub> –0.25	25	0.25	~ 55	2.1	–	–	62	62	277
10	WO <sub>3</sub> –25SiO <sub>2</sub> –0.5	25	0.5	> 90	2.0	667	2.1	60	60	283
11	WO <sub>3</sub> –25SiO <sub>2</sub> –0.75	25	0.75	> 90	1.9	728	3.2	44	44	210
12	WO <sub>3</sub> –25SiO <sub>2</sub> –1	25	1	> 90	2.0	313	5.7	29	29	133

<sup>a</sup> Reaction conditions: 2 mmol cyclooctene, 2 mmol 50 wt% aqueous H<sub>2</sub>O<sub>2</sub>, 1 mmol di-*n*-butyl-ether, 250 mg isopropanol, 2.0 g ethyl acetate, 40 mg catalyst, 80 °C, 4 h.

<sup>b</sup> W loadings determined by ICP-OES analysis (theoretical W loading: 1.97 wt%).

<sup>c</sup> Turnover number (TON), defined as mol<sub>alkene,converted</sub>/mol<sub>W</sub> calculated after 4 h of reaction.

sputter-deposited to improve the conductivity of the sample surface. Fourier Transform infrared spectroscopy (FT-IR) measurements were performed on an IRTracer-100 spectrometer by averaging 64 scans with a spatial resolution of  $4\text{ cm}^{-1}$ . The background spectrum was recorded using an empty cell. Raman spectra were recorded at  $\lambda_{\text{exc}} = 785\text{ nm}$  using a Perkin Elmer Raman Station 400 F at room temperature. The hydrophilicity of the catalysts was evaluated by thermogravimetric analysis (TGA) on a Perkin Elmer TGA 4000 instrument under  $\text{N}_2$  atmosphere with a heating rate of  $10\text{ }^\circ\text{C}/\text{min}$ . The freshly calcined  $\text{WO}_3\text{-SiO}_2$  samples were allowed to reach the maximum degree of water adsorption by an overnight pre-treatment in a desiccator containing a saturated  $\text{NH}_4\text{Cl}$  aqueous solution. The average number of water molecules adsorbed per  $\text{nm}^2$  of the surface of the catalyst was estimated from the mass loss between 25 and  $150\text{ }^\circ\text{C}$  using the following equation [51]:

$$n_{\text{H}_2\text{O}} = \frac{\Delta m}{m_i} \times \frac{N_A}{A_{\text{BET}} M_{\text{H}_2\text{O}}}$$

where  $\Delta m$  is the mass loss between 25 and  $150\text{ }^\circ\text{C}$  (g);  $m_i$  is the initial mass of the sample at  $25\text{ }^\circ\text{C}$  (g);  $N_A$  is the Avogadro constant ( $6.022 \times 10^{23}\text{ mol}^{-1}$ );  $A_{\text{BET}}$  is the specific surface area of the sample ( $\text{nm}^2/\text{g}$ );  $M_{\text{H}_2\text{O}}$  is the molar mass of water ( $18.0153\text{ g/mol}$ ). This measurement was repeated for two times for each material (the deviation was within  $\pm 3\%$ ) and the average values obtained from two tests were reported. X-ray photoelectron spectroscopy (XPS) analysis was performed using a Surface Science SSX-100 ESCA instrument with a monochromatic Al  $K\alpha$  X-ray source ( $h\nu = 1486.6\text{ eV}$ ). Substrates consisting of  $200\text{ nm Au}$  on mica were prepared by sublimation of  $99.99\% \text{ Au}$  (Schöne Edelmetaal B.V.) on freshly cleaved mica, kept previously at  $375\text{ }^\circ\text{C}$  for 16 h in order to remove impurities in a custom-built high-vacuum evaporator (base pressure:  $10^{-7}\text{ mbar}$ ). The sample was deposited on the gold surface by drop-casting and introduced immediately into the spectrometer. The pressure in the measurement chamber was maintained below  $1 \times 10^{-9}\text{ mbar}$ . The electron take-off angle with respect to the surface normal was  $37^\circ$ . The XPS data were acquired by using a spot size of  $600\text{ }\mu\text{m}$  diameter and the energy resolution was set to  $1.3\text{ eV}$  for both the survey spectra and the detailed spectra of the  $\text{W}4f$ ,  $\text{W}4d$ ,  $\text{O}1s$ ,  $\text{Si}2p$  and  $\text{C}1s$  core level regions. During the XPS measurements, an electron flood gun was used to compensate for charging. All XPS spectra were analyzed using the least-squares curve-fitting program Winspec [52]. Deconvolution of the spectra included a Shirley [53] baseline subtraction and fitting with a minimum number of peaks consistent with the chemical structure of the sample, taking into account the experimental resolution. The profile of the peaks was taken as a convolution of Gaussian and Lorentzian functions. Binding energies deduced from fits have an uncertainty of  $\pm 0.1\text{ eV}$  and are referenced to the  $\text{C}1s$  photoemission peak centered at  $284.8\text{ eV}$  [54]. The larger full width at half maximum (FWHM) of the  $\text{W}4d$  signal does not stem from charging effect, as indicated by the absence of an extra component (of the same relative intensity) due to charging in all other XPS peaks. The uncertainty in the peak intensity determination is 2% for all core levels reported. The acidity of the  $\text{WO}_3\text{-}20\text{SiO}_2\text{-}0.5$  catalyst was investigated using FT-IR analysis of adsorbed pyridine. The spectra were recorded on a Bruker Vertex 70 FT-IR spectrometer equipped with a LN-MCT detector in the range  $1400\text{--}1700\text{ cm}^{-1}$ . Each spectrum was collected with a resolution of  $4\text{ cm}^{-1}$ . The sample was prepared in the form of a self-supporting disk. The sample was firstly pre-treated at  $400\text{ }^\circ\text{C}$  for 1 h under reduced pressure ( $0.006\text{ mbar}$ ) and then cooled down to room temperature. During cooling down, the sample reference spectra were recorded at  $350/250/150\text{ }^\circ\text{C}$ . Then, pyridine vapor ( $12\text{ mbar}$ ) was introduced into the system at room temperature for 30 min,

after which the sample was evacuated at room temperature for 30 min to remove physisorbed pyridine. The evacuated samples were subjected to desorption at  $150/250/350\text{ }^\circ\text{C}$  for 30 min, with a heating rate of  $4\text{ }^\circ\text{C}/\text{min}$ , and the FT-IR spectra were recorded at each temperature.

#### 2.4. Catalytic tests

The epoxidation of alkenes with  $\text{H}_2\text{O}_2$  over the  $\text{WO}_3\text{-SiO}_2$  catalysts was carried out in glass vessels (equipped with stirrers and screw caps) that fit into a 48-well high-throughput reaction block equipped with heating and stirring units, which allows performing up to 48 tests simultaneously (Fig. S1B). In a typical catalytic test, 2 mmol alkene, 1 mmol di-*n*-butyl ether (as gas chromatography (GC) internal standard), 250 mg 2-propanol (as cosolvent, to promote the formation of a monophasic liquid reaction mixture) and 2.0 g solvent were firstly weighed in the glass vessel. Then, 2 mmol 50 wt% aqueous  $\text{H}_2\text{O}_2$  and 40 mg  $\text{WO}_3\text{-SiO}_2$  catalyst were added. Then, the glass vial was closed with a screw cap and placed into the 48-well reaction block. Next, the reaction mixture was stirred (800 rpm) at  $80\text{ }^\circ\text{C}$  for 4 h, after which the stirring was stopped and the reaction mixture was centrifuged for 5 min at 4000 rpm to deposit the catalyst. The supernatant was analyzed by means of gas chromatography (GC) using an Agilent Technologies 7980B GC equipped with an Agilent DB-5#6 (5%-phenyl)-methylpolysiloxane column (15 m,  $320\text{ }\mu\text{m}$  ID). The identification of the by-products was performed by GC-mass spectrometry (GC-MS) on an HP 6890 Series GC equipped with a Restek Rxi-5Si MS fused silica column (30 m,  $250\text{ }\mu\text{m}$  ID) coupled to an HP 5973 Mass Selective Detector. The formulae for calculating the moles of substrates obtained from GC measurement and, based on these values, the conversion of alkenes (Conv.), the yield and selectivity (Sel.) towards the epoxides, the turnover number (TON) and turnover frequency (TOF) of the catalyst, the efficiency in the utilization of  $\text{H}_2\text{O}_2$  are listed in the Supporting Information. The catalytic results showed high reproducibility in duplicate tests (deviation in the epoxide yield value within  $\pm 2\%$ ). For these experiments, the average value of the epoxide yield is reported. *Safety note:* hydrogen peroxide and ethers (e.g. 1,4-dioxane and 1,3-dioxolane) can form explosive peroxides unless they contain stabilizers (as it is the case for the ethers used in this work).

Leaching and recycling tests were performed using the optimum catalyst under the optimum reaction conditions. For the leaching test, after reacting at  $80\text{ }^\circ\text{C}$  for 0.5 h, the reaction mixture was centrifuged for 5 min at 4000 rpm to deposit the catalyst. The supernatant was filtered with a  $0.45\text{ }\mu\text{m}$  filter connected to a syringe. Then, a small aliquot of the filtrate was immediately analyzed by GC and the residual liquid was stirred at  $80\text{ }^\circ\text{C}$  for 3.5 h, after which it was also analyzed by GC. The presence or absence of leached active sites was determined from the difference in alkene conversion and epoxide yield between the liquid after 0.5 h and the one after 4 h. For the recycling tests, after reacting at  $80\text{ }^\circ\text{C}$  for 4 h, the catalyst was transferred into a centrifuge tube, deposited by centrifugation at 4000 rpm for 5 min, followed by removal of the supernatant with a pipette. Next, around 40 mL of 1,4-dioxane was added to the centrifuge tube and the tube was shaken vigorously. Then, the tube was centrifuged at 4000 rpm for 30 min, after which the supernatant was removed again. This washing procedure was repeated five times. Then, the catalyst was dried at  $105\text{ }^\circ\text{C}$  for 12 h and regenerated by thermal treatment at  $500\text{ }^\circ\text{C}$  for 3 h (heating rate:  $3\text{ }^\circ\text{C}/\text{min}$ ) before reuse.

The study of the effect of the type of  $\text{H}_2\text{O}_2$  was carried out by comparing the catalytic performance with 50 wt% aqueous  $\text{H}_2\text{O}_2$  to that with 26 wt% anhydrous  $\text{H}_2\text{O}_2$  in ethyl acetate, which was prepared by removing water from the homogeneous solution of

12 mL of 50 wt% aqueous H<sub>2</sub>O<sub>2</sub> and 170 mL of ethyl acetate by means of a Dean-Stark trap at 93 °C. *Safety note:* care should be taken when using anhydrous H<sub>2</sub>O<sub>2</sub> in a flammable organic solvent (explosive) [55]. The Dean-Stark trap was placed in a fume hood to release the oxygen and the possibly explosive gas mixture of oxygen and solvent generated by possible H<sub>2</sub>O<sub>2</sub> decomposition. A rubber cap was placed on top of the condenser instead of a glass cap to prevent the risk of accidents in case of blowing up of the cap caused by pressure build-up from H<sub>2</sub>O<sub>2</sub> decomposition.

### 3. Results and discussion

A novel synthesis method for preparing WO<sub>3</sub>-SiO<sub>2</sub> materials with high specific surface area and highly dispersed W species in the silica matrix was designed by employing supercritical CO<sub>2</sub> as reaction medium. Our approach is based on the use of a tailored reactor that allows the reactants (solutions containing the W and Si precursors and a basic aqueous solution) to come in contact, and thus to form the WO<sub>3</sub>-SiO<sub>2</sub> materials, only in the presence of the scCO<sub>2</sub> medium.

#### 3.1. Synthesis and catalytic testing of the WO<sub>3</sub>-SiO<sub>2</sub> materials

Our study started with the preparation of the WO<sub>3</sub>-SiO<sub>2</sub> materials by a scCO<sub>2</sub>-assisted sol-gel method in which selected synthetic parameters were systematically varied (*i.e.* TMOS concentration and basic solution amount, see Table 1). The nominal loading of WO<sub>3</sub> was kept constant at 2.5 wt% (*i.e.* 2.0 wt% of W). This value was chosen with the aim of preparing materials in which the W loading is sufficiently high to reach a high catalytic activity per gram of material, while granting a high dispersion of the W-based active species in the SiO<sub>2</sub> matrix, which is expected to stabilize them against leaching in the presence of aqueous hydrogen peroxide.

The synthesis of the WO<sub>3</sub>-SiO<sub>2</sub> catalysts with our scCO<sub>2</sub>-assisted method typically gives very high yield of material (> 90% of the theoretical value), although the WO<sub>3</sub>-SiO<sub>2</sub> prepared using the minimum amount of basic solution (Table 1, entries 1, 5, 9) gave lower yield (≤ 55%). This can be explained considering that during the synthesis, after removing CO<sub>2</sub> (*i.e.* at the end of step 3 in Fig. 1), the reaction mixtures prepared using higher amounts of basic solution formed an extensive gel, whereas those prepared with the minimum amount of basic solution consisted of a small amount of gel at the bottom and a viscous supernatant liquid, indicating a lower degree of progress in the hydrolysis-condensation of the precursors. The viscous supernatant containing W or Si species was removed and discarded in the washing step, thus leading to the observed low yield of WO<sub>3</sub>-SiO<sub>2</sub> materials. Additionally, samples from entries 1 and 5 were found to have much higher loading of W compared to the theoretical value (2.0 wt%), indicating that under these conditions the degree of condensation of the Si species was lower compared to the W species.

The prepared WO<sub>3</sub>-SiO<sub>2</sub> materials were tested as heterogeneous catalysts in the epoxidation of cyclooctene with a stoichiometric ratio of H<sub>2</sub>O<sub>2</sub> (1:1) at 80 °C. All the prepared WO<sub>3</sub>-SiO<sub>2</sub> catalysts proved to be active and selective epoxidation catalysts, with the performance varying significantly as a function of the parameters used in the synthesis of the materials (Table 1). When comparing the activity of the WO<sub>3</sub>-SiO<sub>2</sub> catalysts prepared with the same concentration of TMOS solution (*e.g.* Table 1, entries 1–4), the highest cyclooctene conversion was always obtained with the catalyst prepared with the lowest amount of basic solution (base/(W + Si) = 0.25, entries 1, 5, 9). When comparing the activity among WO<sub>3</sub>-SiO<sub>2</sub> catalysts prepared with the same amount of basic solution (*e.g.* Table 1, entries 2, 6, 10), the highest cyclooctene

conversion was always reached over the catalysts prepared with 20 wt% TMOS solution (entries 5–8). Combining these two observations, the WO<sub>3</sub>-20SiO<sub>2</sub>-0.25 catalyst prepared with base/(W + Si) = 0.25 and a 20 wt% TMOS as Si-prec (entry 5) gives the highest cyclooctene conversion (67%). However, this catalyst is not fully selective towards the epoxide product and besides cyclooctene oxide (63% yield), cyclooctane diol was observed as side product (4% yield). The formation of the diol is an indication of the presence of Brønsted acid sites that can catalyze the hydrolysis of the formed epoxide [17]. This is most likely related to the higher W loading present in this catalyst (3.5 wt%), as suggested by the fact that the only other catalyst that led to a non-negligible formation of cyclooctane diol (2%) was WO<sub>3</sub>-15SiO<sub>2</sub>-0.25 (entry 1), which also has a relatively high W loading (4.8 wt%). On the other hand, virtually complete epoxide selectivity (> 99%) was obtained with other WO<sub>3</sub>-SiO<sub>2</sub> catalysts with lower W loadings (around the theoretical value of 2.0 wt%), among which the WO<sub>3</sub>-20SiO<sub>2</sub>-0.5 catalyst (entry 6) gives the highest cyclooctene conversion (62%), with a TON of 278 and a TOF of 70 h<sup>-1</sup>. However, it should be noted that the catalyst prepared with base/(W + Si) = 0.5 and a 25 wt% TMOS as Si-prec (entry 10) displayed an analogous performance. Since the yields in the synthesis of the WO<sub>3</sub>-SiO<sub>2</sub> materials prepared with the minimum amount of basic solution were not optimal and, in the case of WO<sub>3</sub>-15SiO<sub>2</sub>-0.25 and WO<sub>3</sub>-20SiO<sub>2</sub>-0.25, the epoxide selectivity was not complete, these three catalysts were not investigated further (Table 1, entries 1, 5, 9).

To investigate if a lower W loading could be beneficial to the catalytic activity (in terms of TON), a WO<sub>3</sub>-SiO<sub>2</sub> catalyst with a 1.3 wt% WO<sub>3</sub> loading was synthesized. However, the catalytic test over this catalyst gave a much lower cyclooctene conversion and a lower TON than those of the WO<sub>3</sub>-20SiO<sub>2</sub>-0.5 catalyst (for further details, see the Supporting Information). Therefore, it was concluded that a 2.5 wt% WO<sub>3</sub> loading represents the optimum for our scCO<sub>2</sub>-assisted synthesis method. Among the prepared catalysts with this loading, WO<sub>3</sub>-20SiO<sub>2</sub>-0.5 displayed the highest epoxide yield, accompanied with full selectivity and high TON. Therefore, this material was selected for further study.

When employing hydrogen peroxide as oxidant, it is important to estimate to what extent the catalyst is able to promote the desired epoxidation reaction against the competitive decomposition of H<sub>2</sub>O<sub>2</sub> into H<sub>2</sub>O and O<sub>2</sub>. For this purpose, the amount of remaining H<sub>2</sub>O<sub>2</sub> after the test with the WO<sub>3</sub>-20SiO<sub>2</sub>-0.5 catalyst was titrated with a 0.1 M solution of cerium sulfate [Ce(SO<sub>4</sub>)<sub>2</sub>], following a reported protocol [56]. The titration indicated that 13% of the initial amount H<sub>2</sub>O<sub>2</sub> was still present after reaction, which corresponds to a 25% decomposition and thus to a 71% efficiency in the utilization of H<sub>2</sub>O<sub>2</sub>.

Next, the reaction conditions (*i.e.* solvent, H<sub>2</sub>O<sub>2</sub> type) were optimized with the aim of maximizing the epoxide yield over the WO<sub>3</sub>-20SiO<sub>2</sub>-0.5 catalyst. The selected solvent should be able to form a single phase with a mixture of cyclooctene, 50 wt% aqueous H<sub>2</sub>O<sub>2</sub> solution, internal standard and cosolvent, thus avoiding the mass transfer problems that would be associated with a biphasic liquid system. Based on these considerations, a set of solvents (*i.e.* acetonitrile, 1,3-dioxolane, 1,4-dioxane, methanol, ethanol and isopropanol) of either aprotic or protic nature and with different polarities were screened as alternative solvents to ethyl acetate in the epoxidation of cyclooctene with H<sub>2</sub>O<sub>2</sub>, while keeping all other reaction conditions constant. Selected physical properties of these solvents are listed in Table S1. Additionally, solvents with low toxicity, low environmental impact, low flammability and explosion risks are preferable. According to the CHEM21 guide for ranking the safety and greenness of solvents [57], the selected alcohols and ethyl acetate are recommended solvents, acetonitrile is labeled as a problematic solvent, and 1,4-dioxane and 1,3-dioxolane

need to contain stabilizers (as is the case in this work) to avoid being labeled as hazardous solvents due to safety concerns (see experimental section). The catalytic tests clearly indicate that the catalytic activity of  $\text{WO}_3\text{-}20\text{SiO}_2\text{-}0.5$  is higher in aprotic solvents (Fig. 2). The worse performance of protic solvent can be related to the competitive coordination of the protic solvent molecules and  $\text{H}_2\text{O}_2$  to the tungsten centers, which would hinder the activation of  $\text{H}_2\text{O}_2$  [9,58,59]. When comparing the catalytic performance of the  $\text{WO}_3\text{-}20\text{SiO}_2\text{-}0.5$  catalyst as a function of polarity, the activity increased with decreasing dielectric constant value within each class of solvents (aprotic or protic). Highly polar solvents might lead to lower catalytic performance because they can hamper the access of the apolar cyclooctene to the catalyst surface [60]. Combining these two considerations, the  $\text{WO}_3\text{-}20\text{SiO}_2\text{-}0.5$  catalyst demonstrated the highest catalytic activity in terms of cyclooctene conversion (73%), cyclooctene oxide yield (73%) and TON (328) in the most apolar among the tested aprotic solvents (1,4-dioxane).

With the aim of further decreasing the polarity of the reaction mixture, anhydrous  $\text{H}_2\text{O}_2$  (26 wt% in ethyl acetate) was tested as an alternative to aqueous  $\text{H}_2\text{O}_2$ . However, the cyclooctene conversion dropped to 23% under these conditions, which is most likely due to the difficult access of the polar, hydrophilic  $\text{H}_2\text{O}_2$  to the catalyst surface when the latter is covered with an apolar solvent. It can be concluded that the polarity of the reaction mixture should be carefully tuned to ensure a good contact of both alkene and hydrogen peroxide - which have markedly different polarity - with the catalyst surface.

When the catalytic test was performed with half the amount of the  $\text{WO}_3\text{-}20\text{SiO}_2\text{-}0.5$  catalyst (20 mg) in 1,4-dioxane as solvent, a cyclooctene conversion of 35% was obtained, which is around half of that obtained with 40 mg of the  $\text{WO}_3\text{-}20\text{SiO}_2\text{-}0.5$  catalyst (73%), thus excluding external diffusion limitations in the tests performed with 40 mg of catalyst. Importantly, a leaching test with  $\text{WO}_3\text{-}20\text{SiO}_2\text{-}0.5$  proved the true heterogeneity of the catalyst as no further increase of the cyclooctene conversion and epoxide yield was observed after hot-filtration to remove the catalyst after 0.5 h and letting the solution react for further 3.5 h (see Fig. S2). The catalyst was also highly reusable after washing and regeneration by thermal treatment, showing no obvious loss of activity in five consecutive runs (see Fig. S3).

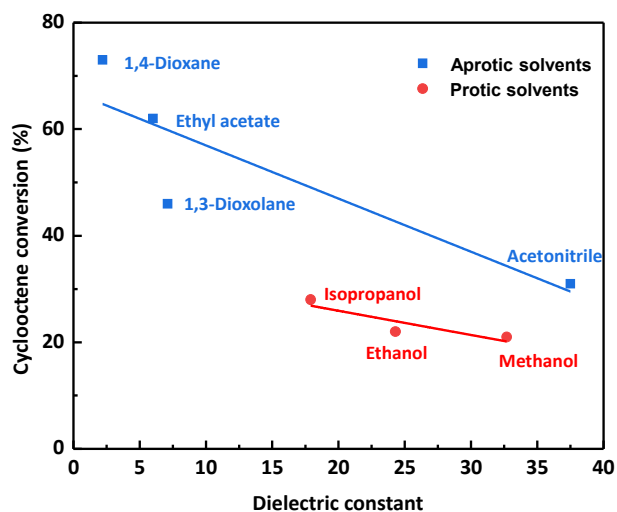


Fig. 2. Cyclooctene conversion over the  $\text{WO}_3\text{-}20\text{SiO}_2\text{-}0.5$  catalyst as a function of the dielectric constant of aprotic (blue) and protic (red) solvents. Reaction conditions as in Table 1.

Additionally, in order to gain more insight on how the  $\text{WO}_3\text{-}20\text{SiO}_2\text{-}0.5$  catalyst activates  $\text{H}_2\text{O}_2$  towards the epoxidation reaction, a control experiment was conducted under the optimum reaction conditions but with the addition of a radical scavenger (TEMPO, 1 mol% relative to  $\text{H}_2\text{O}_2$ ). No difference in cyclooctene oxide yield was observed with or without adding TEMPO, thus indicating that under the employed conditions the  $\text{WO}_3\text{-}20\text{SiO}_2\text{-}0.5$  catalyst follows a non-radical pathway. This strongly suggests that the epoxidation proceeds through the formation of peroxo intermediates (see Scheme 1) over the Lewis acid sites of the  $\text{WO}_3\text{-}20\text{SiO}_2\text{-}0.5$  catalyst, in analogy to several previously reported W-based catalysts for epoxidation reactions [8,15–23].

### 3.2. Catalyst characterization

With the purpose of correlating the good catalytic performance and stability of  $\text{WO}_3\text{-}20\text{SiO}_2\text{-}0.5$  to its physicochemical properties and of comparing it with other  $\text{WO}_3\text{-SiO}_2$  catalysts, we performed a characterization study by a combination of different techniques. The  $\text{N}_2$ -physorption isotherms of all the  $\text{WO}_3\text{-SiO}_2$  materials display a type IV isotherm with a hysteresis loop at high  $p/p^0$  value, indicating the presence of inter-particle void spaces at the mesopore scale in these materials. The isotherm of the optimum catalyst ( $\text{WO}_3\text{-}20\text{SiO}_2\text{-}0.5$ ) is shown in Fig. 3A. The  $\text{WO}_3\text{-}20\text{SiO}_2\text{-}0.5$  catalyst displayed the second highest specific surface area ( $892 \text{ m}^2/\text{g}$ ), slightly lower than that of  $\text{WO}_3\text{-}20\text{SiO}_2\text{-}0.75$  ( $1074 \text{ m}^2/\text{g}$ ), and with both of them being significantly higher than that ( $400 \text{ m}^2/\text{g}$ ) of a  $\text{WO}_3\text{-SiO}_2$  material reported in literature [25], which was prepared with a similar W loading and the same thermal treatment temperature, but in the presence of a template and without  $\text{sCO}_2$ . These results demonstrate that the dispersion of the tungsten species in a silica matrix using our  $\text{sCO}_2$ -assisted method leads to material with high specific surface area, which is a good foundation to grant that a large fraction of the W-sites are exposed on the surface of the material, particularly when compared to unsupported bulk  $\text{WO}_3$  materials (e.g. commercial tungsten oxide,  $\text{WO}_3\text{-Comm}$ , has an extremely low surface area of  $3 \text{ m}^2/\text{g}$ ).

For catalytic applications, the high specific surface area should be ideally combined with a structure that provides unrestricted accessibility to the active sites for reactants and easy removal of the products. In our case, this is proven by TEM analysis, which reveals that  $\text{WO}_3\text{-}20\text{SiO}_2\text{-}0.5$  consists of irregular primary nanoparticles with sizes in the 10–30 nm range (Fig. 4A). In some zones of the TEM images, the nanoparticles form aggregates, though these might not be structural and just be caused by inadequate dispersion of the material in ethanol during the preparation of the TEM sample. Virtually no lattice fringe of crystalline  $\text{WO}_3$  could be found in the sample; an example of the very rare crystalline domains ( $< 10 \text{ nm}$ ) is shown in Fig. S4. The spacing of the magnified lattice fringes is around  $0.384 \text{ nm}$ , which corresponds to the (002) plane of  $\text{WO}_3$  [61]. This observation is in line with the XRD pattern of  $\text{WO}_3\text{-}20\text{SiO}_2\text{-}0.5$  (Fig. 3B), which shows only low-intensity peaks stemming from crystalline  $\text{WO}_3$  at  $23.2^\circ$  and  $33.4^\circ$ , corresponding to the (002) and (022) planes of the monoclinic phase. The broad peak in the  $2\theta = 15\text{--}30^\circ$  range is characteristic for amorphous silica [39]. When comparing the XRD patterns of the  $\text{WO}_3\text{-SiO}_2$  catalysts prepared by our  $\text{sCO}_2$ -assisted method, it can be inferred that the materials with the highest catalytic activity ( $\text{WO}_3\text{-}20\text{SiO}_2\text{-}0.5$  and  $\text{WO}_3\text{-}25\text{SiO}_2\text{-}0.5$ , see Table 1) are also those with the lowest degree of crystallinity (see Fig. S5). This low degree of crystallinity is desirable as it would imply a high dispersion of the W-species and, consequently, a high fraction of W atoms being involved in W–O–Si bonds, which were anticipated to prevent the leaching of W species. The good dispersion of W within the  $\text{WO}_3\text{-}20\text{SiO}_2\text{-}0.5$  material was further proven by elemental mapping with either



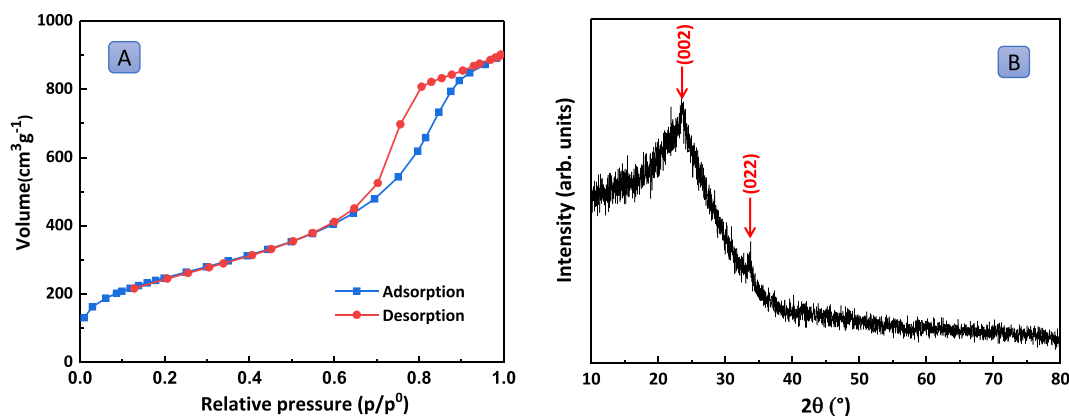


Fig. 3. (A)  $N_2$  adsorption-desorption isotherms and (B) XRD pattern of  $WO_3-20SiO_2-0.5$ .

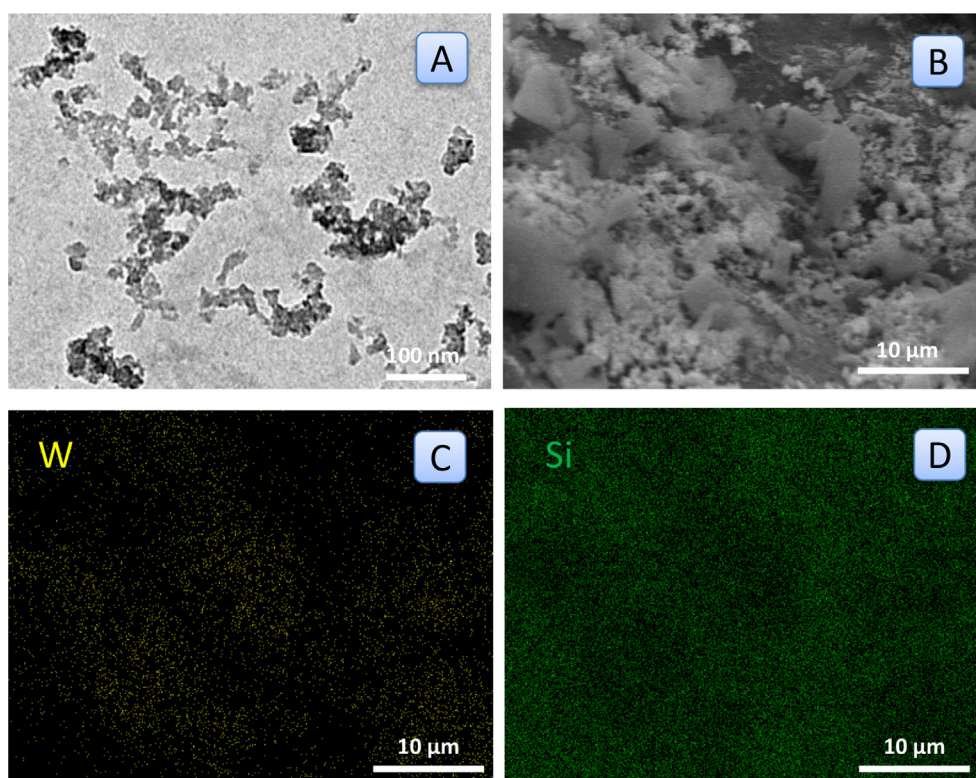


Fig. 4. TEM (A) and SEM (B) images of  $WO_3-20SiO_2-0.5$ . SEM-EDX elemental mapping of W (C) and Si (D).

TEM-EDX (Fig. S4B) or SEM-EDX (Fig. 4B, C, D), which demonstrate a relatively intimate mixing of tungsten and silicon at the nano-scale, although some areas with higher concentration of W than others can be observed at the micrometre scale.

The expected presence of W–O–Si bonds was monitored by FT-IR and Raman spectroscopy. In the FT-IR spectrum of  $WO_3-20SiO_2-0.5$  (Fig. 5A), the prominent peak around  $1041\text{ cm}^{-1}$  ( $\Delta$ ) with a shoulder at around  $1225\text{ cm}^{-1}$  ( $\theta$ ) corresponds to typical stretching vibrations of Si–O–Si bonds [25,29]. The peak at  $802\text{ cm}^{-1}$  ( $\circ$ ) is assigned to the stretching vibrations of Si–O–Si [25,42] and/or W–O–W bonds [40] (as observed in the spectrum of  $WO_3$ -Comm, provided here as a reference). The shoulder at  $963\text{ cm}^{-1}$  ( $\alpha$ ) is ascribed to the vibrations of W species incorporated into silica and is thus an indication of the formation of W–O–Si bonds [25,33].

The broad absorption peak at  $3200\text{--}3600\text{ cm}^{-1}$  is attributed to the –OH stretching vibrations from physisorbed water and surface hydroxyl groups [25]. The small band at  $1610\text{ cm}^{-1}$  ( $\emptyset$ ) is due to the bending mode of physisorbed water [62]. In the Raman spectrum of the  $WO_3-20SiO_2-0.5$  (Fig. 5B), two strong peaks at around  $700\text{ cm}^{-1}$  ( $\ddot{o}$ ) and  $800\text{ cm}^{-1}$  ( $\bullet$ ) correspond to the stretching modes of W–O–W [63]. The positions of these peaks are shifted compared to those in the Raman spectrum of  $WO_3$ -Comm due to the incorporation of these  $WO_3$  domains into the silica matrix. In the range of  $200\text{--}400\text{ cm}^{-1}$ , the spectrum of  $WO_3$ -Comm displays two separate bands for the bending vibrations of O–W–O bond at  $270\text{ cm}^{-1}$  ( $*$ ) and  $328\text{ cm}^{-1}$  ( $\#$ ) [63], while the spectrum of  $WO_3-20SiO_2-0.5$  exhibits a broad peak in this range that is ascribed to the incorporation of W species in silica [24,34,42,64].

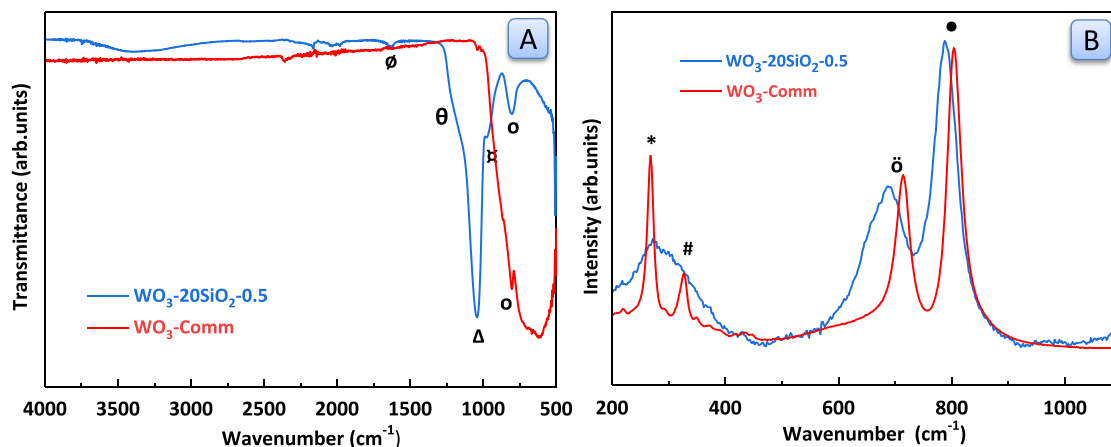


Fig. 5. (A) FT-IR spectra of  $\text{WO}_3\text{-}20\text{SiO}_2\text{-}0.5$  and  $\text{WO}_3\text{-Comm}$ . (B) Raman spectra of  $\text{WO}_3\text{-}20\text{SiO}_2\text{-}0.5$  and  $\text{WO}_3\text{-Comm}$ .

Next, XPS analysis was conducted in order to shed light on the oxidation state of tungsten (V or VI) and on the chemical composition of  $\text{WO}_3\text{-}20\text{SiO}_2\text{-}0.5$ . The wide-scan spectrum of  $\text{WO}_3\text{-}20\text{SiO}_2\text{-}0.5$  (Fig. S6 and Table S2) shows the expected presence of Si and O as main constituent elements of the sample, together with 2.4 wt% W, in good agreement with the loading obtained by ICP-OES analysis (2.1 wt%). The XPS signals of the W4f and W4d core levels are shown in Fig. 6 and Fig. S7. Although the W4f signal is typically used to study tungsten by XPS [65–67], here the W4d core level was also considered, for the purpose of analyzing the oxidation state of tungsten. As illustrated in the Supporting Information (Fig. S7), two doublets were required in the fitting of the W4f signal. The first one peaked at a binding energy (BE) of 36.9 eV (red in Fig. 6A) and is ascribed to  $\text{W}^{\text{VI}}$ , while the doublet at lower BE (blue in Fig. 6A), i.e. peaking at 35.4 eV, is assigned to  $\text{W}^{\text{V}}$  [66–69]. Both doublets are shifted towards higher BE with respect to the results reported in previous studies [66–69]. Such a shift has been attributed to tungsten linked by a chemical bond to the  $\text{SiO}_2$  matrix [65]. The W4d signal shows two peaks at BEs of 248.3 eV and 261.1 eV (Fig. 6B), which correspond to the spin-orbit split components  $\text{W}4d_{5/2}$  and  $\text{W}4d_{3/2}$ , respectively. Their separation is 12.8 eV, suggesting a  $\text{W}^{\text{VI}}$  oxidation state [70]. However, like for the W4f signal, a good fit of the W4d signal requires two doublets

corresponding to the two oxidation states: for the  $\text{W}4d_{5/2}$  peak the component peaking at 248.7 eV is due to  $\text{W}^{\text{VI}}$  (red in Fig. 6B) and the component at lower binding energy (blue in Fig. 6B), can be assigned to  $\text{W}^{\text{V}}$  [69,71,72]. Also in this case, the shift of the two doublets towards higher binding energy can be ascribed to the chemical bond between tungsten and the  $\text{SiO}_2$  matrix. The XPS signals of the O1s and Si2p core levels did not provide additional information on the W species (see Figs. S8–S10). In summary, the XPS analysis indicates that both  $\text{W}^{\text{VI}}$  and  $\text{W}^{\text{V}}$  species are present in  $\text{WO}_3\text{-}20\text{SiO}_2\text{-}0.5$ , and that their relative abundance is similar within the experimental uncertainty (see Table S3).

For W-based epoxidation catalysts, it has been reported that weak Lewis acid sites catalyze the formation of the epoxide product, while Brønsted acid sites promote the formation of the diol [17]. The nature, strength and amount of the acid sites of  $\text{WO}_3\text{-}20\text{SiO}_2\text{-}0.5$  was characterized by monitoring the characteristic FT-IR-absorption peaks related to the adsorption of pyridine on Lewis acid sites and on Brønsted acid sites, as a function of temperature (Fig. 7) [63]. The peaks at  $1452\text{ cm}^{-1}$  and  $1614\text{ cm}^{-1}$  are assigned to the characteristic vibration modes of coordinated pyridine on strong Lewis acid sites (which persist upon desorption at  $200\text{ }^\circ\text{C}$ ), while the peaks at  $1577\text{ cm}^{-1}$  and  $1596\text{ cm}^{-1}$  are related to

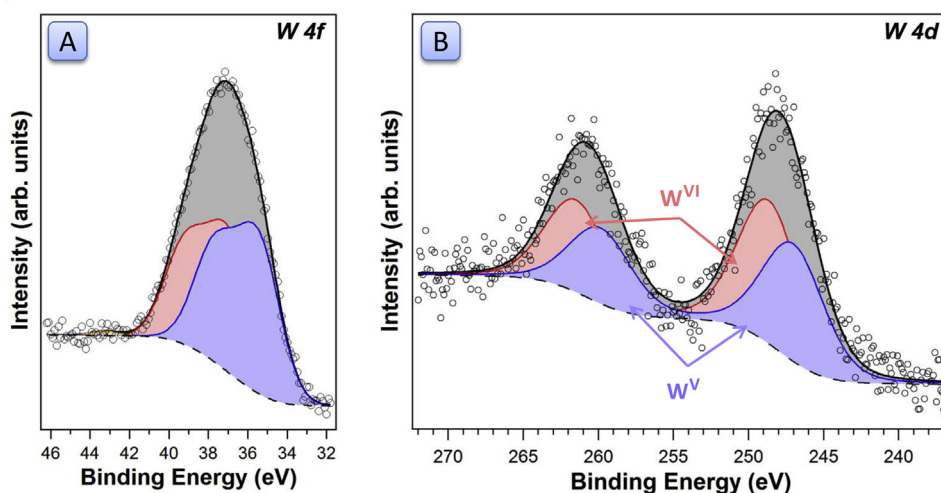


Fig. 6. XPS signals of: (A) W4f and (B) W4d core levels of  $\text{WO}_3\text{-}20\text{SiO}_2\text{-}0.5$  and corresponding fits. Two doublet functions were used to deconvolute the W4f signal. The (spin-orbit) splitting energy is  $(2.2 \pm 0.1)$  eV. The small shoulder at higher binding energy, i.e. 43.2 eV, represents the  $\text{W}5p_{3/2}$  core level. In the deconvolution of the W4d signal, the (spin-orbit) energy splitting is  $(12.8 \pm 0.1)$  eV.

the vibration modes of coordinated pyridine on weak Lewis acid sites. The peaks at  $1540\text{ cm}^{-1}$  are ascribed to the vibration mode of pyridinium ions on Brønsted acid sites [40,42]. Based on the integrated absorbance of Lewis/Brønsted acid bands and molecular absorption coefficients [73], the concentrations of Lewis and Brønsted acid sites were estimated to be 42.3 and 1.3  $\mu\text{mol/g}$ , respectively. These results indicate that the  $\text{WO}_3\text{-}20\text{SiO}_2\text{-}0.5$  catalyst possesses mainly Lewis acid sites, which are the proposed active sites for the epoxidation (Scheme 1), alongside with a small fraction of Brønsted acid sites. These Lewis and Brønsted acid sites can originate from both  $\text{W}^{\text{VI}}$  and  $\text{W}^{\text{V}}$  species coordinated to a silica matrix [74,75]. For each oxidation state, the Lewis acid sites display a higher degree of coordination to Si atoms compared to Brønsted acid sites (Fig. 8). Therefore, the larger fraction of Lewis acid sites observed in our catalyst can be ascribed to the good dispersion of the W sites in the silica matrix that was indicated by XRD, TEM, SEM-EDX and XPS (*vide supra*) and that stems from our  $\text{sCO}_2$ -assisted method. This hypothesis is also supported by the fact that the total amount of acids determined by FT-IR of adsorbed pyridine (43.6  $\mu\text{mol/g}$ ) corresponds to 40% of the W atoms present in  $\text{WO}_3\text{-}20\text{SiO}_2\text{-}0.5$  (108  $\mu\text{mol/g}$ ).

Finally, the surface hydrophilicity of the  $\text{WO}_3\text{-SiO}_2$  catalysts was evaluated on the basis of their ability to adsorb water molecules as monitored by TGA (see Table 1). It is important to tune the surface hydrophilicity of catalysts for the epoxidation of alkenes with  $\text{H}_2\text{O}_2$  to ensure a good contact with both apolar alkene and polar  $\text{H}_2\text{O}_2$  [51]. When comparing the surface hydrophilicity among  $\text{WO}_3\text{-SiO}_2$  materials prepared with the same concentration of TMOS solution, those prepared employing lower amounts of basic solution are less hydrophilic. When comparing  $\text{WO}_3\text{-SiO}_2$  catalysts synthesized with the same amount of basic solution, those prepared with a higher concentration of TMOS are less hydrophilic. The two most active catalysts identified in this work ( $\text{WO}_3\text{-}20\text{SiO}_2\text{-}0.5$  and  $\text{WO}_3\text{-}25\text{SiO}_2\text{-}0.5$ ) are also the two with lowest hydrophilicity.

Based on the above characterization results, the superior catalytic activity of  $\text{WO}_3\text{-}20\text{SiO}_2\text{-}0.5$  is attributed to a combination of its physicochemical properties: (i) the presence of accessible W species acting as Lewis acid sites; (ii) the high specific surface area ( $892\text{ m}^2/\text{g}$ ) and non-porous, and thus non-confined, open structure of the nanoparticles, which enhance the number and accessibility of catalytic sites; (iii) the relatively low hydrophilicity of its surface, which can facilitate contact with both cyclooctene and  $\text{H}_2\text{O}_2$  while avoiding strong bonding of water, which may poison the active sites

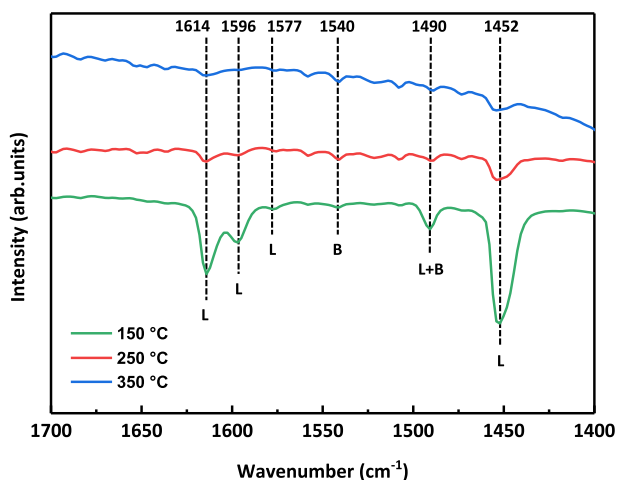


Fig. 7. FT-IR spectra of adsorbed pyridine on the  $\text{WO}_3\text{-}20\text{SiO}_2\text{-}0.5$  catalyst, recorded at different temperatures.

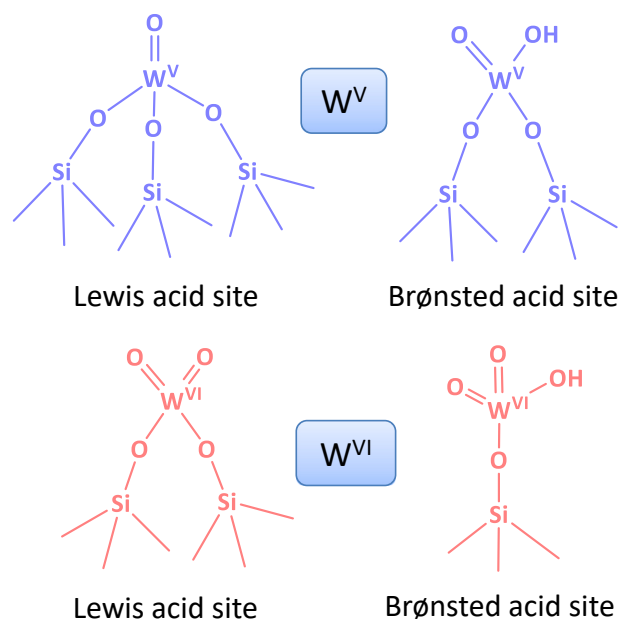


Fig. 8. Proposed models of the structures of  $\text{W}^{\text{V}}$  and  $\text{W}^{\text{VI}}$  species in the  $\text{WO}_3\text{-}20\text{SiO}_2\text{-}0.5$  catalyst.

[55]; (iv) the good dispersion of W species within the silica matrix, which implies that a large fraction of the W atoms are acting as catalytic sites (the number of accessible Lewis acid sites corresponds to 39% of the total W atoms present in the material) while preventing their leaching and thus granting the observed good reusability of  $\text{WO}_3\text{-}20\text{SiO}_2\text{-}0.5$ .

### 3.3. Comparison with other catalysts

The activity of the  $\text{WO}_3\text{-}20\text{SiO}_2\text{-}0.5$  catalyst prepared with the  $\text{sCO}_2$ -assisted sol-gel method was compared with that of a reference catalyst prepared via a similar sol-gel route but without  $\text{sCO}_2$  ( $\text{WO}_3\text{-SiO}_2\text{-Ref}$ ) and of bulk  $\text{WO}_3$  ( $\text{WO}_3\text{-Comm}$ ). The  $\text{WO}_3\text{-SiO}_2\text{-Ref}$  catalyst showed lower cyclooctene conversion (55%) and epoxide yield (55%). It also suffered from leaching of active species (see leaching test result in Fig. S2), which is caused by the existence of large  $\text{WO}_3$  particles ( $> 50\text{ nm}$ ) in the material, as proved by TEM-EDX analysis (Fig. S11). On the other hand, these large  $\text{WO}_3$  particles are absent in  $\text{WO}_3\text{-}20\text{SiO}_2\text{-}0.5$ , which also possesses a higher specific surface area ( $892\text{ m}^2/\text{g}$ ) than  $\text{WO}_3\text{-SiO}_2\text{-Ref}$  ( $826\text{ m}^2/\text{g}$ ). The structural differences between these two catalysts indicate the importance of employing  $\text{sCO}_2$  in the sol-gel synthesis for achieving good dispersion of W species in the silica matrix, high surface area and, consequently, a good catalytic performance in terms of both activity and stability. The second reference catalyst,  $\text{WO}_3\text{-Comm}$ , displayed a lower but still appreciable cyclooctene conversion (44%) with virtually complete epoxide selectivity, despite the extremely low specific surface area ( $3\text{ m}^2/\text{g}$ ). This is consistent with literature reports that show that bulk  $\text{WO}_3$  contains Lewis acid sites that contribute in catalyzing the epoxidation of alkenes [23,29]. The difference in the amount of W between  $\text{WO}_3\text{-}20\text{SiO}_2\text{-}0.5$  and  $\text{WO}_3\text{-Comm}$  was taken into account by calculating and comparing the TON based on W content. The TON number obtained with  $\text{WO}_3\text{-}20\text{SiO}_2\text{-}0.5$  catalyst is almost two orders of magnitude larger than that for  $\text{WO}_3\text{-Comm}$  (328 vs. 5), demonstrating the importance of dispersing the W species in the high surface area  $\text{WO}_3\text{-}20\text{SiO}_2\text{-}0.5$ .

Further evaluation of the performance of the  $\text{WO}_3\text{-}20\text{SiO}_2\text{-}0.5$  catalyst can be obtained by comparison with state-of-the-art W-based heterogeneous catalysts for the epoxidation of cyclooctene with  $\text{H}_2\text{O}_2$  reported in the literature (see Table S4 for an overview). Although the TOF of our optimum catalyst ( $82\text{ h}^{-1}$ ) is lower compared to those of  $\text{WO}_3$  nanoparticles ( $140\text{ h}^{-1}$ ) [23] and  $\text{W-Zn-SnO}_2$  ( $147\text{ h}^{-1}$ ) [76], the synthesis of  $\text{WO}_3\text{-}20\text{SiO}_2\text{-}0.5$  is more environmental friendly as it does not require the use of high temperature as in flame spray pyrolysis or Sn as raw material. Additionally, the recovery of  $\text{WO}_3\text{-}20\text{SiO}_2\text{-}0.5$  is easier compared to the very small  $\text{WO}_3$  nanoparticles (average size of 13 nm). A remarkable higher TOF was obtained over  $\text{WO}_3\text{-SiO}_2$  ( $1648\text{ h}^{-1}$ ) [43], though only an 8 min reaction was carried out and no leaching test was performed. On the other hand, the TOF of  $\text{WO}_3\text{-}20\text{SiO}_2\text{-}0.5$  is much higher compared to those of  $\text{WO}_3\text{-MCM-}48$  ( $4\text{ h}^{-1}$ ) [28],  $\text{W-MMM-E}$  ( $33\text{ h}^{-1}$ ) [34] or  $\text{W-MCM-}41$  ( $3\text{ h}^{-1}$ ) [35], though these catalysts were tested at lower reaction temperatures, and the leaching of  $\text{WO}_3\text{-MCM-}48$  was not addressed while the latter two catalysts suffered from leaching problems. Although a thorough comparison is hindered by the difference in reaction conditions, the catalytic performance of  $\text{WO}_3\text{-}20\text{SiO}_2\text{-}0.5$  in the epoxidation of cyclooctene with  $\text{H}_2\text{O}_2$  in terms of conversion, epoxide yield, TON and TOF is also remarkable when compared to state-of-the-art heterogeneous catalysts based on other metal species (e.g. Ti, Ga, Nb) dispersed in a silica matrix (see Table S5).

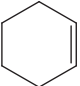
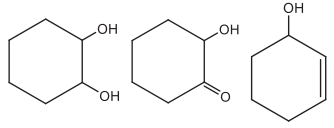
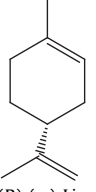
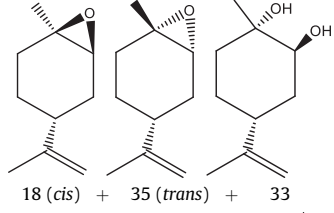
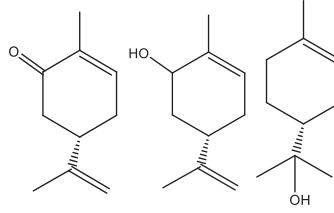
### 3.4. Substrate scope

Another aspect that we investigated was the versatility of the  $\text{WO}_3\text{-}20\text{SiO}_2\text{-}0.5$  catalyst, which was explored by expanding the substrate scope to other unsaturated compounds, e.g. cyclohexene and limonene. Cyclohexene oxide is industrially used to prepare cyclohexane diol, an important platform chemical in the synthesis of pharmaceutical products, polyester resins, and liquid crystals

[41,77,78]. The internal oxide of limonene can find application in the synthesis of biodegradable polycarbonate by  $\text{CO}_2$  addition [79,80], while the di-oxide of limonene can be employed as a reactive diluent in cationic UV-curing or as a monomer for the production of polyurethanes [55]. Under the optimum reaction conditions (see Table 2), the  $\text{WO}_3\text{-}20\text{SiO}_2\text{-}0.5$  catalyst was able to convert 84% of cyclohexene, with cyclohexane diol as the main product (78% Sel.) and 2-hydroxy-cyclohexene-1-one (17% Sel., formed by the oxidation of the diol) and 2-cyclohexene-1-ol (5% Sel., formed by the oxidation of the allylic C–H bond of cyclohexene) as side products. No epoxide was observed, in contrast with the high epoxide selectivity observed with cyclooctene (*vide supra*), which stems from the higher stability of cyclooctene oxide [1,81]. The hydrolysis of the epoxide ring leading to the formation of the diol is catalyzed by Brønsted acid sites.  $\text{WO}_3\text{-}20\text{SiO}_2\text{-}0.5$  displays mainly Lewis acidity (*vide supra*) and has only a relatively small population of Brønsted acid sites. However, the FT-IR spectra of adsorbed pyridine (Fig. 7) show that the intensity of the signal related to Brønsted acid sites does not decrease significantly by increasing temperature, proving the strong nature of these sites. Therefore, the formation of the diol is attributed to the strength rather than to the number of Brønsted acid sites in  $\text{WO}_3\text{-}20\text{SiO}_2\text{-}0.5$ .

The conversion of limonene over the  $\text{WO}_3\text{-}20\text{SiO}_2\text{-}0.5$  catalyst reached 54% with a 53% epoxide selectivity under the employed reaction conditions (see Table 2). Among the epoxide products, only the internal epoxide was observed (18% Sel. towards *cis*-internal-oxide; 35% Sel. towards *trans*-internal-oxide), with no terminal epoxide or diepoxide being found. This is ascribed to the electrophilic attack of the oxygen atom from the activated  $\text{H}_2\text{O}_2$ , which occurs preferentially on the more electron-rich internal C=C bond [82], and to the use of a 1:1 ratio between  $\text{H}_2\text{O}_2$  and limonene (compared to the 2:1 ratio that would be needed for the theoretical complete conversion of two C=C bonds in limonene). The corresponding diol (33% Sel.) was formed as the main side product,

**Table 2**  
Epoxidation of cyclohexene and (R)-(+)-limonene catalyzed by  $\text{WO}_3\text{-}20\text{SiO}_2\text{-}0.5^a$

Substrate	Conv. (%)	Product Sel. (%)
 Cyclohexene	84	 78 + 17 + 5
 (R)-(+)-Limonene	54	 18 ( <i>cis</i> ) + 35 ( <i>trans</i> ) + 33  5 + 3 + 1 + trace amounts of other side products (5)

<sup>a</sup> Reaction conditions: 2 mmol substrate, 2 mmol  $\text{H}_2\text{O}_2$  (50 wt% in aqueous solution), 1 mmol di-*n*-butyl-ether, 250 mg isopropanol, 2.0 g 1,4-dioxane, 40 mg  $\text{WO}_3\text{-}20\text{SiO}_2\text{-}0.5$  catalyst,  $80^\circ\text{C}$ , 4 h.

which is also related to the presence of Brønsted acid sites on the  $\text{WO}_3\text{-}20\text{SiO}_2\text{-}0.5$  catalyst. Minor amounts of three other side products (5% carvone + 3% carveol + 1% terpineol) were also detected. There were a few side products with trace amounts (5% in total) that could not be identified by GC-MS.

#### 4. Conclusions

In this work,  $\text{WO}_3\text{-SiO}_2$  with a high specific surface area ( $892\text{ m}^2/\text{g}$ ) and good dispersion of W species was prepared by a novel, template-free supercritical- $\text{CO}_2$ -assisted sol-gel method. For this purpose, a tailored reactor set-up was designed and employed to allow the formation of the  $\text{WO}_3\text{-SiO}_2$  materials to take place only in the presence of supercritical  $\text{CO}_2$  medium. The method was used to synthesize a series of  $\text{WO}_3\text{-SiO}_2$  materials by systematic variation of selected synthetic parameters (TMOS concentration, aqueous ammonia solution, W precursor amount, applying supercritical condition or not). The obtained  $\text{WO}_3\text{-SiO}_2$  materials were applied as heterogeneous catalysts for the epoxidation of alkenes with  $\text{H}_2\text{O}_2$  as oxidant. The most active catalyst was not the material with the highest specific surface area ( $1034\text{ m}^2/\text{g}$ ) but the one combining a high specific surface area ( $892\text{ m}^2/\text{g}$ ) with good dispersion of tungsten species within the silica matrix (as evidenced by XRD, TEM, SEM-EDX and XPS) and relatively low surface hydrophilicity (TGA). The W species display mainly Lewis acid character, thus providing the active sites for the epoxidation, with only a minor fraction of Brønsted acid sites (as shown by FT-IR analysis of adsorbed pyridine). The optimum catalyst ( $\text{WO}_3\text{-}20\text{SiO}_2\text{-}0.5$ ) achieved 73% cyclooctene conversion with > 99% epoxide selectivity at  $80\text{ }^\circ\text{C}$  after 4 h, employing a stoichiometric ratio of  $\text{H}_2\text{O}_2$  (1:1) in 1,4-dioxane as solvent. Importantly, the common problem associated with the leaching of W species when employing W-based heterogeneous catalysis in the presence of water was prevented by preparing  $\text{WO}_3\text{-SiO}_2$  with this synthesis method. This is ascribed to the formation of W-O-Si bond in our material, as proved by FT-IR, Raman, and XPS analysis. The catalyst was reused in five consecutive runs (after washing and thermal treatment) with no loss of activity. Notably, the catalyst is also versatile as it was active in the conversion of cyclohexene to cyclohexane diol and in the transformation of limonene to limonene oxide. Additionally, our novel  $\text{scCO}_2$ -assisted sol-gel method has the potential to be extended to the synthesis of other silica-based materials in which metals and silica are homogeneously distributed rather than forming separate domains.

#### Data availability

All data presented in this work are stored according to the Research Data Management Plan of the University of Groningen and are available upon request.

#### Author contributions

**Yehan Tao:** Investigation; Methodology; Formal analysis; Validation; Writing; Visualization.

**Oreste De Luca:** Investigation; Formal analysis; Writing; Visualization.

**Bhawan Singh:** Methodology; Resources; Supervision.

**Aeilke J. Kamphuis:** Methodology; Resources; Supervision.

**Juan Chen:** Investigation; Formal analysis.

**Petra Rudolf:** Formal analysis; Supervision; Writing.

**Paolo P. Pescarmona:** Conceptualization; Methodology; Formal analysis; Supervision; Writing; Visualization; Project administration.

#### Declaration of competing interest

The authors declare that they have no known competing financial interests or personal relationships that could have appeared to influence the work reported in this paper.

#### Acknowledgements

We are thankful for TEM support from Dr. Marc A. Stuart, Raman spectroscopy support from Prof. Wesley Browne, ICP-OES support from Hans van der Velde, analytical support from Léon Rohrbach and technical support from Marcel de Vries and Erwin Wilbers. Yehan Tao acknowledges financial support from the China Scholarship Council (CSC) for her Ph.D. grant.

#### Appendix A. Supplementary data

Supplementary data to this article can be found online at <https://doi.org/10.1016/j.mtchem.2020.100373>.

#### References

- [1] I. Arends, R. Sheldon, Recent developments in selective catalytic epoxidations with  $\text{H}_2\text{O}_2$ , *Top. Catal.* 19 (2002) 133–141.
- [2] G. Grigoropoulou, J. Clark, J. Elings, Recent developments on the epoxidation of alkenes using hydrogen peroxide as an oxidant, *Green Chem.* 5 (2003) 1–7.
- [3] X. Huali, F. Yongxian, Z. Chunhui, D. Zexue, M. Enze, G. Zhonghua, L. Xiaonian, A new, efficient route to titanium-silsesquioxane epoxidation catalysts developed by using high-speed experimentation techniques, *Chem. Biochem. Eng. Q.* 22 (2008) 25–39.
- [4] R. Noyori, M. Aoki, K. Sato, Sustainability in catalytic oxidation: an alternative approach or a structural evolution? *Chem. Commun.* (2003) 1977–1986.
- [5] B.S. Lane, K. Burgess, Metal-catalyzed epoxidations of alkenes with hydrogen peroxide, *Chem. Rev.* 103 (2003) 2457–2474.
- [6] D.E. De Vos, B.F. Sels, P.A. Jacobs, Practical heterogeneous catalysts for epoxide production, *Adv. Synth. Catal.* 345 (2003) 457–473.
- [7] M.G. Clerici, O.A. Kholdeeva, *Liquid Phase Oxidation via Heterogeneous Catalysis: organic synthesis and industrial applications*, John Wiley & Sons, 2013.
- [8] S.-S. Wang, G.-Y. Yang, Recent advances in polyoxometalate-catalyzed reactions, *Chem. Rev.* 115 (2005) 4893–4962.
- [9] A. Corma, P. Esteve, A. Martinez, Solvent effects during the oxidation of olefins and alcohols with hydrogen peroxide on Ti-beta catalyst: the influence of the hydrophilicity-hydrophobicity of the zeolite, *J. Catal.* 161 (1996) 11–19.
- [10] V. Elias, M. Crivello, E. Herrero, S. Casuscelli, G. Eimer, Synthesis of titanium-containing mesoporous silicas as catalysts for cyclohexene epoxidation, *Ind. Eng. Chem. Res.* 48 (2009) 9076–9082.
- [11] M. Guidotti, C. Pirovano, N. Ravasio, B. Lazaro, J. Fraile, J. Mayoral, B. Coq, A. Galarneau, The use of  $\text{H}_2\text{O}_2$  over titanium-grafted mesoporous silica catalysts: a step further towards sustainable epoxidation, *Green Chem.* 11 (2009) 1421–1427.
- [12] K. Lin, O.I. Lebedev, G. Van Tendeloo, P.A. Jacobs, P.P. Pescarmona, Titanosilicate beads with hierarchical porosity: synthesis and application as epoxidation catalysts, *Chem. Eur. J.* 16 (2010) 13509–13518.
- [13] F. Chiker, F. Launay, J. Nogier, J. Bonardet, Green and selective epoxidation of alkenes catalysed by new  $\text{TiO}_2\text{-SiO}_2$  SBA mesoporous solids, *Green Chem.* 5 (2003) 318–322.
- [14] K. Lin, P.P. Pescarmona, K. Houthoofd, D. Liang, G. Van Tendeloo, P.A. Jacobs, Direct room-temperature synthesis of methyl-functionalized Ti-MCM-41 nanoparticles and their catalytic performance in epoxidation, *J. Catal.* 263 (2009) 75–82.
- [15] N. Mizuno, K. Yamaguchi, K. Kamata, Epoxidation of olefins with hydrogen peroxide catalyzed by polyoxometalates, *Coord. Chem. Rev.* 249 (2005) 1944–1956.
- [16] N. Mizuno, K. Kamata, K. Yamaguchi, Green oxidation reactions by polyoxometalate-based catalysts: from molecular to solid catalysts, *Top. Catal.* 53 (2010) 876–893.
- [17] W. Yan, G. Zhang, H. Yan, Y. Liu, X. Chen, X. Feng, X. Jin, C. Yang, Liquid-phase epoxidation of light olefins over W and Nb nanocatalysts, *ACS Sustain. Chem. Eng.* 6 (2018) 4423–4452.
- [18] C. Venturello, R. D'Aloisio, J.C. Bart, M. Ricci, A new peroxotungsten heteropoly anion with special oxidizing properties: synthesis and structure of tetrahexylammonium tetra (diperoxotungsto) phosphate (3-), *J. Mol. Catal.* 32 (1985) 107–110.
- [19] Y. Ishii, K. Yamawaki, T. Ura, H. Yamada, T. Yoshida, M. Ogawa, Epoxidation of olefins and allylic alcohols, ketonization of alcohols and diols, and oxidative cleavage of 1, 2-diols and olefins, *J. Org. Chem.* 53 (1988) 3587–3593.

- [20] K. Kamata, R. Ishimoto, T. Hirano, S. Kuzuya, K. Uehara, N. Mizuno, Epoxidation of alkenes with hydrogen peroxide catalyzed by selenium-containing dinuclear peroxotungstate and kinetic, spectroscopic, and theoretical investigation of the mechanism, *Inorg. Chem.* 49 (2010) 2471–2478.
- [21] K. Kamata, K. Yonehara, Y. Sumida, K. Yamaguchi, S. Hikichi, N. Mizuno, Efficient epoxidation of olefins with  $\geq 99\%$  selectivity and use of hydrogen peroxide, *Science* 300 (2003) 964–966.
- [22] K. Kamata, K. Sugahara, K. Yonehara, R. Ishimoto, N. Mizuno, Efficient epoxidation of electron-deficient alkenes with hydrogen peroxide catalyzed by  $[\gamma\text{-PW}_{10}\text{O}_{38}\text{V}_2(\mu\text{-OH})_2]^{3-}$ , *Chem. Eur. J.* 17 (2011) 7549–7559.
- [23] C. Hammond, J. Straus, M. Righettoni, S.E. Pratsinis, I. Hermans, Nanoparticulate tungsten oxide for catalytic epoxidations, *ACS Catal.* 3 (2013) 321–327.
- [24] C. Martín, P. Malet, G. Solana, V. Rives, Structural analysis of silica-supported tungstates, *J. Phys. Chem. B* 102 (1998) 2759–2768.
- [25] F. Adam, A. Iqbal, The liquid phase oxidation of styrene with tungsten modified silica as a catalyst, *Chem. Eng. J.* 171 (2011) 1379–1386.
- [26] R. Gao, X. Yang, W.-L. Dai, Y. Le, H. Li, K. Fan, High-activity, single-site mesoporous  $\text{WO}_3$ -MCF materials for the catalytic epoxidation of cycloocta-1,5-diene with aqueous hydrogen peroxide, *J. Catal.* 256 (2008) 259–267.
- [27] L. Mädler, H. Kammler, R. Mueller, S.E. Pratsinis, Controlled synthesis of nanostructured particles by flame spray pyrolysis, *J. Aerosol Sci.* 33 (2002) 369–389.
- [28] D.H. Koo, M. Kim, S. Chang,  $\text{WO}_3$  nanoparticles on MCM-48 as a highly selective and versatile heterogeneous catalyst for the oxidation of olefins, sulfides, and cyclic ketones, *Org. Lett.* (2005) 5015–5018.
- [29] R. Bera, S. Koner, Incorporation of tungsten oxide in mesoporous silica: catalytic epoxidation of olefins using sodium-bi-carbonate as co-catalyst, *Inorg. Chim. Acta.* 384 (2012) 233–238.
- [30] G. Gelbard, T. Gauducheau, E. Vidal, V.I. Parvulescu, A. Crosman, V.M. Pop, Epoxidation with peroxotungstic acid immobilised onto silica-grafted phosphoramides, *J. Mol. Catal. Chem.* 182 (2002) 257–266.
- [31] J. Jarupatrakorn, M. Coles, T. Tilley, Synthesis and characterization of  $\text{MO}[\text{OSi}(\text{O}^i\text{Bu})_3]_4$  and  $\text{MO}_2[\text{OSi}(\text{O}^i\text{Bu})_3]_2$  ( $\text{M} = \text{Mo}, \text{W}$ ): models for isolated oxomolybdenum and-tungsten sites on silica and precursors to molybdena- and Tungsta- silica materials, *Chem. Mater.* 17 (2005) 1818–1828.
- [32] C. Bisio, A. Gallo, R. Psaro, C. Tiozzo, M. Guidotti, F. Carniato, Tungsten-oxide-grafted silica catalysts for the selective epoxidation of alkenes, *Appl. Catal. Gen.* 581 (2019) 133–142.
- [33] X.-L. Yang, W.-L. Dai, H. Chen, Y. Cao, H. Li, H. He, K. Fan, Novel efficient and green approach to the synthesis of glutaraldehyde over highly active W-doped SBA-15 catalyst, *J. Catal.* 229 (2005) 259–263.
- [34] N. Maksimchuk, I. Ivanchikova, O. Zalomaeva, Y. Chesalov, A. Shmakov, V. Zaikovskii, O. Kholdeeva, Tungsten-based mesoporous silicates W-MMM-E as heterogeneous catalysts for liquid-phase oxidations with aqueous  $\text{H}_2\text{O}_2$ , *Catalysts* 8 (2018) 95.
- [35] E. Briot, J.-Y. Piquemal, M. Vennat, J.-M. Brégeault, G. Chottard, J.-M. Manoli, Aqueous acidic hydrogen peroxide as an efficient medium for tungsten insertion into MCM-41 mesoporous molecular sieves with high metal dispersion, *J. Mater. Chem.* 10 (2000) 953–958.
- [36] S. Maksasithorn, P. Praserttham, K. Suriye, M. Devillers, D.P. Debecker,  $\text{WO}_3$ -based catalysts prepared by non-hydrolytic sol-gel for the production of propene by cross-metathesis of ethene and 2-butene, *Appl. Catal. Gen.* 488 (2014) 200–207.
- [37] B. Hu, H. Liu, K. Tao, C. Xiong, S. Zhou, Highly active doped mesoporous KIT-6 catalysts for metathesis of 1-Butene and ethene to propene: the influence of neighboring environment of W species, *J. Phys. Chem. C* 117 (2013) 26385–26395.
- [38] Y. Tao, P. Pescarmona, Nanostructured oxides synthesised via scCO<sub>2</sub>-assisted sol-gel methods and their application in catalysis, *Catalysts* 8 (2018) 212.
- [39] G. Liu, X. Wang, X. Wang, H. Han, C. Li, Photocatalytic  $\text{H}_2$  and  $\text{O}_2$  evolution over tungsten oxide dispersed on silica, *J. Catal.* 293 (2012) 61–66.
- [40] A. Kunal, M. Dongare, S. Umbarkar, Sol-gel synthesised  $\text{WO}_3$  nanoparticles supported on mesoporous silica for liquid phase nitration of aromatics, *Appl. Catal. B Environ.* 182 (2016) 142–152.
- [41] P. Bhaumik, P. Kane, P.L. Dhepe, Silica and zirconia supported tungsten, molybdenum and gallium oxide catalysts for the synthesis of furfural, *Catal. Sci. Technol.* 4 (2014) 2904–2907.
- [42] P. Bhaumik, P.L. Dhepe, From lignocellulosic biomass to furfural: insight into the active species of a silica-supported tungsten oxide catalyst, *ChemCatChem* 9 (2017) 2709–2716.
- [43] F. Somma, G. Strukul, Oxidation of geraniol and other substituted olefins with hydrogen peroxide using mesoporous, sol-gel-made tungsten oxide-silica mixed oxide catalysts, *J. Catal.* 227 (2004) 344–351.
- [44] Z. Novak, P. Kotnik, Z. Knez, Preparation of  $\text{WO}_3$  aerogel catalysts using supercritical  $\text{CO}_2$  drying, *J. Non-Cryst. Solids* 350 (2004) 308–313.
- [45] S. Bozbag, D. Sanli, C. Erkey, Synthesis of nanostructured materials using supercritical  $\text{CO}_2$ : Part II. Chemical transformations, *J. Mater. Sci.* 47 (2012) 3469–3492.
- [46] J. Jammaer, C. Aprile, S.W. Verbruggen, S. Lenaerts, P.P. Pescarmona, J.A. Martens, A non-aqueous synthesis of  $\text{TiO}_2/\text{SiO}_2$  composites in supercritical  $\text{CO}_2$  for the photodegradation of pollutants, *ChemSusChem* 4 (2011) 1457–1463.
- [47] R. Sui, A.S. Rizkalla, P.A. Charpentier, Formation of titania nanofibers: a direct sol-gel route in supercritical  $\text{CO}_2$ , *Langmuir* 21 (2005) 6150–6153.
- [48] M.E. Tadros, C.L. Adkins, E.M. Russick, M.P. Youngman, Synthesis of titanium dioxide particles in supercritical  $\text{CO}_2$ , *J. Supercrit. Fluids* 9 (1996) 172–176.
- [49] J. Choi, C.B. Shin, T.-J. Park, D.J. Suh, Characteristics of vanadia-titania aerogel catalysts for oxidative destruction of 1, 2-dichlorobenzene, *Appl. Catal. Gen.* 311 (2006) 105–111.
- [50] X. Xia, R. Jin, Y. He, J.-F. Deng, H. Li, Surface properties and catalytic behaviors of  $\text{WO}_3/\text{SiO}_2$  in selective oxidation of cyclopentene to glutaraldehyde, *Appl. Surf. Sci.* 165 (2000) 255–259.
- [51] W. Lueangchaichaweng, N.R. Brooks, S. Fiorilli, E. Gobechiya, K. Lin, L. Li, S. Parres-Esclapez, E. Javon, S. Bals, G. Van Tendeloo, Gallium oxide nanorods: novel, template-free synthesis and high catalytic activity in epoxidation reactions, *Angew. Chem. Int. Ed.* 53 (2014) 1585–1589.
- [52] N. Lise, Laboratory of the Facultés Universitaires Notre-Dame de la Paix, Belgium.
- [53] D.A. Shirley, High-resolution X-ray photoemission spectrum of the valence bands of gold, *Phys. Rev. B* 5 (1972) 4709.
- [54] J. Moulder, W. Stickle, P. Sobol, Handbook of X-Ray Photoelectron Spectroscopy, Perkin-Elmer, Physical Electronics Division, 1993.
- [55] W. Lueangchaichaweng, B. Singh, D. Mandelli, W.A. Carvalho, S. Fiorilli, P.P. Pescarmona, High surface area, nanostructured boehmite and alumina catalysts: synthesis and application in the sustainable epoxidation of alkenes, *Appl. Catal. Gen.* 571 (2019) 180–187.
- [56] P.P. Pescarmona, K.P. Janssen, P.A. Jacobs, Novel Transition-metal-free heterogeneous epoxidation catalysts discovered by means of high-throughput experimentation, *Chem. Eur. J.* 13 (2007) 6562–6572.
- [57] D. Prat, A. Wells, J. Hayler, H. Sneddon, C.R. McElroy, S. Abou-Shehadeh, P.J. Dunn, CHEM21 selection guide of classical-and less classical-solvents, *Green Chem.* 18 (2015) 288–296.
- [58] G. Grivani, V. Tahmasebi, A.D. Khalaji, K. Fejfarová, M.J.P. Dušek, Synthesis, characterization and crystal structure determination of a new vanadium (IV) Schiff base complex (VOL2) and investigation of its catalytic activity in the epoxidation of cyclooctene, *Polyhedron* 51 (2013) 54–60.
- [59] M. Mirzaee, B. Bahramian, J. Gholizadeh, A. Feizi, R.J.C.E.J. Gholami, Acetylacetonate complexes of vanadium and molybdenum supported on functionalized boehmite nano-particles for the catalytic epoxidation of alkenes, *Chem. Eng. J.* 308 (2017) 160–168.
- [60] P.P. Pescarmona, P.A. Jacobs, A high-throughput experimentation study of the epoxidation of alkenes with transition-metal-free heterogeneous catalysts, *Catal. Today* 137 (2008) 52–60.
- [61] J.Y. Zheng, A.U. Pawar, C.W. Kim, Y.J. Kim, Y.S. Kang, Highly enhancing photoelectrochemical performance of facilely-fabricated Bi-induced (002)-oriented  $\text{WO}_3$  film with intermittent short-time negative polarization, *Appl. Catal. B Environ.* 233 (2018) 88–98.
- [62] A.T. Bolsoni, J.S. Dos Santos, M.D. Assis, H.P. Oliveira, Synthesis, characterization, and catalytic properties of a mesostructured lamellar xerogel tungsten oxide phase, *J. Non-Cryst. Solids* 357 (2011) 3301–3306.
- [63] M. Daniel, B. Desbat, J. Lassegues, B. Gerard, M.J. Figlarz, Infrared and Raman study of  $\text{WO}_3$  tungsten trioxides and  $\text{WO}_3 \cdot x\text{H}_2\text{O}$  tungsten trioxide hydrates, *J. Solid State Chem.* 67 (1987) 235–247.
- [64] W.P. Griffith, T. Wickins, Raman studies on species in aqueous solutions. Part II. Oxy-species of metals of groups VI A, VA, and IV A, *J. Chem. Soc. Inorg. Phys. Theor.* (1967) 675–679.
- [65] F. Verpoort, L. Fiermans, A. Bossuyt, L. Verdonck, Olefin metathesis catalyst. Part I. Angle-resolved and depth profiling XPS study of tungsten oxide on silica, *J. Mol. Catal.* 90 (1994) 43–52.
- [66] J. Zhu, M. Vasilopoulou, D. Davazoglou, S. Kennou, A. Chroneos, U. Schwingenschlög, Intrinsic defects and H doping in  $\text{WO}_3$ , *Sci. Rep.* 7 (2017) 40882.
- [67] M. Feng, A. Pan, H. Zhang, Z. Li, F. Liu, H. Liu, D. Shi, B. Zou, H. Gao, Strong photoluminescence of nanostructured crystalline tungsten oxide thin films, *Appl. Phys. Lett.* 86 (2005) 141901.
- [68] P. Biloen, G. Pott, X-ray photoelectron spectroscopy study of supported tungsten oxide, *J. Catal.* 30 (1973) 169–174.
- [69] G. McGuire, G.K. Schweitzer, T.A. Carlson, Core electron binding energies in some Group IIIA, VB, and VIB compounds, *Inorg. Chem.* 12 (1973) 2450–2453.
- [70] Y. Cai, Y. Wang, S. Deng, G. Chen, Q. Li, B. Han, R. Han, Y. Wang, Graphene nanosheets-tungsten oxides composite for supercapacitor electrode, *Ceram. Int.* 40 (2014) 4109–4116.
- [71] C.W. Lai, S. Sreekantan, Effect of heat treatment on  $\text{WO}_3$ -loaded  $\text{TiO}_2$  nanotubes for hydrogen generation via enhanced water splitting, *Mater. Sci. Semicond. Process.* 16 (2013) 947–954.
- [72] D. Sarma, C. Rao, XPS studies of oxides of second-and third-row transition metals including rare earths, *J. Electron. Spectrosc.* 20 (1980) 25–45.
- [73] C.A. Emeis, Determination of integrated molar extinction coefficients for infrared absorption bands of pyridine adsorbed on solid acid catalysts, *J. Catal.* 141 (1993) 347–354.
- [74] X. Yang, W. Dai, R. Gao, K. Fan, Characterization and catalytic behavior of highly active tungsten-doped SBA-15 catalyst in the synthesis of glutaraldehyde using an anhydrous approach, *J. Catal.* 249 (2007) 278–288.
- [75] X. Yang, R. Gao, W. Dai, K. Fan, Influence of tungsten precursors on the structure and catalytic properties of  $\text{WO}_3/\text{SBA-15}$  in the selective oxidation of cyclopentene to glutaraldehyde, *J. Phys. Chem. C* 112 (2008) 3819–3826.
- [76] K. Kamata, K. Yonehara, Y. Sumida, K. Hirata, S. Nojima, N. Mizuno, Efficient heterogeneous epoxidation of alkenes by a supported tungsten oxide catalyst, *Angew. Chem. Int. Ed.* 50 (2011) 12062–12066.

- [77] L. Yu, J. Wang, T. Chen, Y. Wang, Q. Xu, Recyclable 1,2-bis[3,5-bis (trifluoromethyl) phenyl] diselane-catalyzed oxidation of cyclohexene with H<sub>2</sub>O<sub>2</sub>: a practical access to trans-1,2-cyclohexanediol, *Appl. Organomet. Chem.* 28 (2014) 652–656.
- [78] T. Maschmeyer, M.C. Klunduk, C.M. Martin, D.S. Shephard, J. Thomas, B.F. Johnson, Modelling the active sites of heterogeneous titanium-centred epoxidation catalysts with soluble silsesquioxane analogues, *Chem. Commun.* (1997) 1847–1848.
- [79] A.J. Bonon, Y.N. Kozlov, J.O. Bahú, R. Maciel Filho, D. Mandelli, G.B. Shul'pin, Limonene epoxidation with H<sub>2</sub>O<sub>2</sub> promoted by Al<sub>2</sub>O<sub>3</sub>: kinetic study, experimental design, *J. Catal.* 319 (2014) 71–86.
- [80] C.M. Byrne, S.D. Allen, E.B. Lobkovsky, G.W. Coates, Alternating copolymerization of limonene oxide and carbon dioxide, *J. Am. Chem. Soc.* 126 (2004) 11404–11405.
- [81] C. Antonetti, A.M.R. Galletti, P. Accorinti, S. Alini, P. Babini, K. Raabova, E. Rozhko, A. Caldarelli, P. Righi, F. Cavani, P. Concepcion, Two alternative routes for 1, 2-cyclohexanediol synthesis by means of green processes: cyclohexene dihydroxylation and catechol hydrogenation, *Appl. Catal. Gen.* 466 (2013) 21–31.
- [82] A. Feliczak-Guzik, I. Nowak, Mesoporous niobosilicates serving as catalysts for synthesis of fragrances, *Catal. Today* 142 (2009) 288–292.